Genetic variation associated with plastic and homeostatic growth responses to drought in Arabidopsis

Running head: Adaptive homeostasis in Arabidopsis drought response

Ángel Ferrero-Serrano[1*] & Sarah M. Assmann[1*]

[1]Biology Department, Penn State University, 208 Mueller Laboratory, University Park, PA, 16802, USA

*** Correspondence:**

Ángel Ferrero-Serrano: aaf11@psu.edu

Sarah M. Assmann: sma3@psu.edu

Highlight

Information on phenotype, genotype, and transcript abundance is integrated to identify candidate plasticity and homeostasis genes and processes associated with local adaptation to drought stress in Arabidopsis accessions of the Iberian Peninsula.

Abstract

Natural genetic variation influences plant responses to environmental stressors. However, the extent to which such variation underlies plastic versus homeostatic response phenotypes deserves more attention. We quantified the extent of drought-induced changes in leaf area in a set of Iberian Arabidopsis accessions and then performed association studies correlating plasticity and homeostasis in this phenotype with genomic and transcriptomic variation. Drought-induced plastic reductions in relative leaf area typified accessions originating from productive environments. In contrast, homeostasis in relative leaf area typified accessions originating from unproductive environments. Genome-Wide Association Studies (GWAS), Transcriptome Wide Association Studies (TWAS), and expression GWAS (eGWAS) highlighted the importance of auxin-related processes in conferring leaf area plasticity. Homeostatic responses in relative leaf area were associated with a diverse gene set and positively associated with a higher intrinsic water use efficiency (WUE_i), as confirmed in a TWAS metanalysis of previously published $\delta^{13}C$ measurements. Thus, we have identified not only candidate "plasticity genes" but also candidate "homeostasis genes" controlling leaf area. Our results exemplify the value of a combined GWAS, TWAS, and eGWAS approach to identify mechanisms underlying phenotypic responses to stress.

Keywords: *Arabidopsis thaliana* (Arabidopsis), drought, eGWAS, GWAS, plasticity, transcriptome, TWAS, WUE_i.

Introduction

In the Italian novel The Leopard, one of the main characters famously conveys the idea that 'Everything must change so that everything can stay the same.' Often, there is a cost associated with change that resonates with the plastic developmental responses observed in plants when faced with stress (Bradshaw, 1965; West-Eberhard, 2003). Plasticity marks a departure from a homeostatic state in response to an environmental cue, often followed by "allostatic" responses to return to a homeostatic state (Fig. 1). These allostatic responses involve a myriad of physiological and developmental regulatory processes that stabilize critical aspects of plant physiology. Under repeated stress there is an associated metabolic and physiological cost associated with departure from the optimal state that is not completely alleviated upon return to homeostasis. These retained detrimental

53 effects are known as allostatic load (McEwen and Stellar, 1993), with important implications for
54 fitness and survival from an evolutionary standpoint.

55 Stress often elicits plastic responses in plant developmental traits (Dorn *et al.*, 2000; van
56 Kleunen and Fischer, 2005; Forsman, 2015). However, simply because a given trait is plastic does
57 not mean that this plasticity is adaptive (Ghalambor *et al.*, 2007). Plants that are not adapted to stress
58 may exhibit plastic responses that are maladaptive. Under such conditions, homeostasis or lack of
59 plasticity may, in turn, be adaptive (Fig. 1; Ferrero-Serrano and Chakravorty, 2023). This study aims
60 to explore the genetic basis of both plasticity and homeostasis imposed by recurrent drought events
61 during the vegetative development of *Arabidopsis thaliana*.

62 Drought is among the strongest factors driving adaptation in plants (Siepielski *et al.*, 2017;
63 Exposito-Alonso *et al.*, 2019). Since climate projections predict drought events to become more
64 frequent, intense, and unpredictable (Donat *et al.*, 2016), we can expect that drought episodes will
65 become increasingly more difficult for plants to adapt to. For this reason, understanding the genetic
66 basis and adaptation potential of phenotypic traits and their plastic or homeostatic responses to
67 drought is paramount for ameliorating climate change impacts in natural and managed ecosystems.

68 The Iberian Peninsula is a drought-prone region particularly vulnerable to the effects of
69 climate change on precipitation (Vicente-Serrano, 2006a; Vicente-Serrano, 2006b; Coll *et al.*, 2016;
70 Páscoa *et al.*, 2017). The Iberian Arabidopsis population is particularly valuable because its
71 accessions originate from a broad range of environments (Lobo *et al.*, 2001; Rey Benayas and
72 Scheiner, 2002), and previous studies of this population have provided considerable insight into
73 Arabidopsis evolution and development (Picó *et al.*, 2008; Montesinos *et al.*, 2009; Gomaa *et al.*,
74 2011; Méndez-Vigo *et al.*, 2011; Montesinos-Navarro *et al.*, 2011; Picó, 2012; Manzano-Piedras *et*
75 *al.*, 2014; Wolfe and Tonsor, 2014; Vidigal *et al.*, 2016; Exposito-Alonso *et al.*, 2018a; Marcer *et al.*,
76 2018; Castilla *et al*. 2020). In the present study, we utilize GWAS, Transcriptome-Wide Association
77 Studies (TWAS), and Expression Genome-Wide Association Studies (eGWAS) to identify natural
78 genetic and transcript abundance variation underlying both plastic and homeostatic leaf area
79 responses to drought in Iberian Arabidopsis accessions. Leaf area is a vital trait in relation to growth:
80 leaf area production determines the total amount of light intercepted by plants, carbon assimilation,
81 and the extent of evaporative water loss. We uncover an adaptive homeostatic growth strategy in
82 accessions from less productive environments, address its genetic basis, and conclude that phenotypic

homeostasis is under genetic control and of evolutionary importance, just as previously argued for plasticity (Bradshaw, 1965; Via *et al.*, 1995).

Materials and Methods

Plant materials and phenotyping

Seeds for 43 Iberian accessions (Table P1 for the list of accessions) were cold-stratified for four days at 4°C to synchronize germination. Plants were grown in 10 cm square pots containing Metro-mix 360 potting mixture (Sun Gro Horticulture Canada Ltd) in a greenhouse with an average daytime 500 μmol $m^{-2}s^{-1}$ photosynthetic photon flux density (PPFD) (8h light: 16h dark, with light supplied as natural daylight supplemented with 1000W metal halide lamps) and average day/night temperatures of 22°C /20°C.

For each Iberian accession, we grew one plant per pot, with five replicates for each of the control and drought treatments (10 plants for each individual accession), for a total of 430 plants (43 accessions × (five control + five droughted plants)). This is a greater number of replicates than for many association studies (Seren *et al.*, 2020). Both control and drought treatment were well-watered for the first 28 days, maintaining the soil relative water content at field capacity as measured by monitoring pot weight daily and adding water when necessary. After 28 days, soil in the drought treatment was allowed to dry down. These pots were then rewatered to soil saturation once every 10 days for a total of 14 drought cycles until the conclusion of the experiment, 175 days after seeds were sown. Here, as in the natural environments we sought to mimic, the soil water content was not adjusted based on the size of individual plants. Our protocol simulated the natural recurring cycle of rainfall and drought. Such cycles are often used in studies of natural variation (i.e. Exposito-Alonso *et al.*, 2018b; Exposito-Alonso *et al.*, 2019) and in field trials on crop cultivars (IRRI, 2021). In contrast, the well-watered treatment was maintained near field capacity throughout the experiment. Plants were spatially randomized within the greenhouse every week throughout the experiment. At the end of the experiment, nine accessions within the drought treatment with mortality rates higher than 40% (i.e., at least two of the five replicates; Table P1) were excluded from downstream analyses.

Photographs of the rosettes were taken at the time of flowering and subsequently analyzed using ImageJ (http://imagej.nih.gov/ij/) to determine the projected leaf area for each accession under both well-watered and drought treatments (Fig. S1; Table P1).

Determination of relative leaf area and plasticity

Relative leaf area (rLA) is defined here as the leaf area (LA) at the time of flowering for each accession under each experimental condition (either well-watered or drought) relative to all the accessions under the same condition. The relative leaf area of a given accession under well-watered conditions ($rLA_{i\ (well\text{-}watered)}$) is thus calculated as:

$$rLA_{i\ (well-watered)} = \frac{LA_{i\ (well-watered)}}{LA_{m\ (well-watered)}}$$

where $LA_{i\ (well\text{-}watered)}$ is the leaf area of any individual accession, and $LA_{m\ (well\text{-}watered)}$ is the average leaf area for all accessions grown under the same conditions. Similarly, the relative leaf area under drought ($rLA_{i\ (drought)}$) for each accession is calculated as:

$$rLA_{i\ (drought)} = \frac{LA_{i\ (drought)}}{LA_{m\ (drought)}}$$

where $LA_{i\ (drought)}$ is the leaf area of any individual accession under drought and $LA_{m\ (drought)}$ is the average value for all accessions when grown under drought. A high rLA reflects greater vegetative growth of any given accession relative to the set of accessions utilized in this study. The use of rLA, rather than actual values, was essential to allow a normalized comparison of the leaf area of each accession between the watering regimes. Reaction norms based on rLA were employed to quantify plastic changes in relative leaf area between the two treatments (well-watered vs. drought). Leaf area plasticity indexes were calculated based on an established definition (Weijschedé *et al.*, 2006). The leaf area plasticity index to drought (PI) was calculated for each accession as follows:

$$PI = rLA_{i\ (drought)} - rLA_{i\ (well-watered)}$$

A positive leaf area plasticity index does not necessarily imply that the leaf area for that accession was higher under drought, but rather that under drought, a given accession displays a higher rLA relative to the rest of accessions in the study.

Genome-wide association study

Genome-Wide Association Studies (GWAS) identify genetic variants associated with natural variation in a phenotypic trait of interest. We used a GWAS approach to identify polymorphisms associated with natural variation in rLA and its plasticity. The online tool GWAPP (http://gwas.gmi.oeaw.ac.at/) was employed using a linear regression model (Seren *et al.*, 2012). The

143 linear regression model does not address the confounding effects of population stratification, family
144 structure, and cryptic relatedness (Price *et al.*, 2010); however, these issues are minimized by our
145 choice of a regional (Iberian) population (Frachon *et al.*, 2018; Tabas-Madrid *et al.*, 2018; Frachon
146 *et al.*, 2019). Nonetheless, we demonstrate that the candidate SNPs discussed here were also
147 significant after the application of a mixed model approach implemented either using GWAPP (Seren
148 *et al.*, 2012) or GWAS-Flow (Freudenthal *et al.*, 2019) (Figs S2, S3, and S4; Tables G1-G6),
149 providing further confidence in our results.

150 We filtered out low-frequency variants (minor allele frequency (MAF) < 10%) to focus on
151 variants less likely to be undergoing negative selection or to be spurious SNPs from sequencing
152 errors. We obtained gene model annotation from the TAIR11 genome release. We defined the
153 'consensus' transcript variant as the variant producing the longest transcript. We predicted the effect
154 of every SNP using SnpEff (Cingolani *et al.*, 2012). We focused on SNPs within gene transcriptional
155 units, including introns, untranslated regions at the 5′ and 3′ ends, and open reading frames, as defined
156 in Araport11 (Cheng *et al.*, 2017). We also included the promoter region, defined as 5 kb upstream
157 of the most distal transcription start site. We imposed a stringent arbitrary significance threshold
158 corresponding to a score of four ($P < 0.0001$; Fig. S5A-E).

159 Using the results from GWAS obtained from the association with rLA, we obtained reaction
160 norms that reflect plastic or homeostatic patterns of genome-wide associations of these traits in
161 response to drought. The association between a phenotype and any given SNP was designated as
162 homeostatic if it was found significantly associated with that trait under both conditions (well-watered
163 and drought).

164

165 **Transcriptome-wide association**

166 Natural variation in gene expression is an important mechanism of local adaptation (Des Marais *et*
167 *al.*, 2012; Lasky *et al.,* 2014). Transcriptome-Wide Association Studies (TWAS) identify variation
168 in transcript abundance associated with observed variation in phenotypic traits (Gusev *et al.*, 2016;
169 Kremling *et al.*, 2019). TWAS analysis does not suffer from the limitations imposed by false non-
170 causal synthetic associations due to linkage disequilibrium (Li *et al.*, 2021) that are typical of GWAS
171 (Korte and Farlow 2013). Also, TWAS evaluates continuous variation in transcript abundance rather
172 than the discrete presence/absence of SNPs with (potentially) additive or synergistic effects on a
173 continuous phenotype. We retrieved the transcriptome data from rosette leaves of 727 Arabidopsis

174 accessions from the GEO dataset with accession number GSE80744 and SRA study SRP074107
175 (Kawakatsu *et al.*, 2016) and subsetted the 35 Iberian accessions that overlapped with the 43 Iberian
176 accessions used in our study. Data wrangling was conducted utilizing the dplyr (Wickham *et al.*,
177 2015) and tidyr (Wickham and Henry, 2018) packages. Spearman's rank correlation coefficients
178 between the variation in individual phenotypic values (relative leaf area (rLA_i), plasticity index (PI),
179 and intrinsic water use efficiency (WUE_i) from Dittberner *et al.* (2018; Tables P1 and P2)), and
180 individual transcript abundance values within the study population, were calculated using the
181 correlation function of the Hmisc package (Harrell Jr and Dupont, 2019). The stronger the association
182 of the two variables, the closer the Pearson's correlation coefficient, r_s, will be to either +1 or -1. We
183 imposed a threshold based on this correlation coefficient ($|r_s| \geq 4.0$). We considered this threshold to
184 be stringent after inspection of the distribution of the results (Fig. S5F-J). We include the r_s and
185 corresponding *P*-values in Tables T1 and T2.
186 Using the results from TWAS, we derived reaction norms to reflect homeostatic patterns of
187 transcriptome-wide associations of rLA in response to drought. Any given transcript was designated
188 homeostatic if found significantly associated with rLA (either positively or negatively; $|r_s| \geq 4.0$)
189 under both conditions (well-watered and drought).
190

191 **eGWAS**

192 Natural variation in transcript abundance can also be used to identify candidate SNPs (expression
193 SNPs or eSNPs) that control transcript abundance in an Expression Genome-Wide Association Study
194 (eGWAS). eGWAS was conducted by compiling the transcript abundance values of a given gene of
195 interest, extracting the transcript abundance for that particular gene in the 727 Arabidopsis accessions
196 from the GEO dataset with accession number GSE80744 and SRA study SRP074107 (Kawakatsu *et*
197 *al.*, 2016), then subsetting the 665 accessions included in the 1001 Genomes project (The 1001
198 Genomes Consortium, 2016). Then, the online tool GWAPP (http://gwas.gmi.oeaw.ac.at/) was
199 employed using a linear regression model (Seren *et al.*, 2012) to identify candidate regulatory
200 variants. Regulatory variants are either cis- or trans-acting, depending on the location of the genetic
201 variant. cis-eSNPs were defined as those located within the ORF, introns, UTRs, or the promoter
202 region of the regulated gene. Trans-eSNPs were defined as those located within the ORF, introns,
203 UTRs, or promoter region of a gene different from the gene transcriptionally regulated by that genetic
204 variant.

Analyses

AraCLIM (https://github.com/CLIMtools/) is a database that describes the local environment of the Arabidopsis accessions sequenced as part of the 1001 Genomes Project (Ferrero-Serrano and Assmann, 2019; Ferrero-Serrano et al., 2022). We obtained from AraCLIM the values for MOD17A2 (Net Primary Productivity in the spring season) (Heinsch *et al.*, 2003; Running and Zhao, 2015) at the collection site of each accession and evaluated the correlation with the phenotypes obtained in our experiment.

WUE_i is defined as the ratio between instantaneous carbon gain and transpirational water loss, typically calculated per unit of leaf area (Condon *et al.*, 2002). To integrate information from previously published studies on the Iberian Arabidopsis population, we retrieved available data on natural variation in intrinsic water use efficiency (WUE_i, $\delta^{13}C$), previously recorded by Dittberner *et al.* (2018). During photosynthesis, plants discriminate against $^{13}CO_2$ in the reaction center of *Ribulose 1, 5-biphosphate carboxylase/oxidase* (*RuBisCO*). As stomata close, minimizing water loss in response to drought, the discrimination against $^{13}CO_2$ decreases because the internal CO_2 concentration (C_i) becomes unavoidably reduced. As a result of their reduced C_i, plants with greater WUE_i experience lower CO_2 concentrations at the sites of carboxylation (C_c) and have less negative $\delta^{13}C$ values.

All statistical analyses and figures were produced using R (Team, 2013). The code and data to reproduce the analysis, figures, and tables are available at https://github.com/AssmannLab and Zenodo. Gene Ontology (GO) biological process analysis (Tables GO1-GO10) was performed using the open-source software ShinyGO v0.61: http://bioinformatics.sdstate.edu/go60/ (Ge *et al.*, 2020) with the following settings: the search species was "*Arabidopsis thaliana*," the *P*-value cutoff (FDR) was 0.05, and the number of most significant terms to show was ten. To replicate these results, the lists of genes that were input into these analyses based on significance thresholds can be selected from Tables G1-G6, T1, and T2. Each analytical technique used in this study has assumptions and limitations, which we discuss in Document S1. The code and data necessary to reproduce all analyses and figures in this study are available on GitHub (https://github.com/AssmannLab).

232 **Results**

233 **Natural variation in leaf area and plasticity in response to long-term cyclical**
234 **drought**

235 To quantify phenotypic variation in Iberian Arabidopsis accessions exposed to drought, we conducted
236 a common garden experiment (Fig. 2A). We used image analysis to derive rosette leaf area under
237 well-watered or drought conditions (Figs 2B, S1; Table P1). As expected, we observed a significant
238 ($P < 0.001$) reduction in leaf area resulting from drought in most genotypes, as evidenced by the
239 phenotypic reaction norms. In contrast, a small number of accessions exhibited constant or increased
240 leaf area under drought (Fig. 2B; Table P1), demonstrating that a reduction in leaf area in drought is
241 not inescapable. Based on these data, we calculated the relative leaf area (rLA) of each accession
242 under both well-watered and drought conditions (see Materials & Methods; Fig. 2C; Table P1). We
243 used rLA rather than the actual leaf area to allow comparison of the leaf area of each accession relative
244 to the study population for each watering regime. We also show that the plasticity index derived from
245 the difference in rLA between conditions (i.e. reflecting the slopes of the reaction norms in Fig. 2C;
246 Table P1) is proportional to the fold change in leaf area under drought relative to well-watered
247 conditions (Fig. S6).

248 We explored the relationship between rLA in the absence of drought and its plastic response
249 (plasticity index; PI) to drought. Fig. 2D shows that in general accessions with higher rLA under
250 well-watered conditions displayed greater plastic reductions in rLA when subjected to drought
251 (negative leaf area plasticity; yellow datapoints in Figs 2D, E). However, this relationship was not
252 invariant; we also observed individual accessions with high rLA under well-watered conditions and
253 positive plasticity indexes under drought (green datapoints in Fig. 2D and Fig. 2E). Moreover a few
254 accessions displayed low rLA and negative leaf area plasticity indexes (red datapoints in Fig. 2D and
255 Fig. 2E), Most commonly, accessions with lower rLA under well-watered conditions displayed
256 homeostatic phenotypic responses to drought (Fig. 2D, E blue datapoints).

257

258 While the severity of drought depends on multiple environmental parameters, its
259 physiological response is very characteristic. It results in stomatal closure and a reduction in CO_2
260 assimilation, as reflected in decreases in Net Primary Productivity (NPP), an index that, therefore,
261 can be used as a reliable drought indicator (Huang *et al.*, 2016). We determined that the plastic leaf

262 area responses (negative values of leaf area plasticity index) we observed in our study were typical
263 of accessions from more productive habitats as reflected in Net Primary Productivity in spring (NPP
264 spring; Fig. 3A). In contrast, homeostatic leaf area responses (zero or positive values of leaf area
265 plasticity index) were typical of accessions from less productive habitats (Fig. 3A).

266 Genetic variants significantly associated with leaf area plasticity were identified by GWAS
267 (Fig. 3B; Table G3). Gene ontology (GO) analysis of functions associated with the genes harboring
268 the variants identified by GWAS revealed an enrichment in auxin-related processes (Table GO1).
269 Among the variants identified from GWAS (Fig. 3B; Table G3) as associated with leaf area plasticity,
270 we highlight two co-varying SNPs in the 5' and 3' UTR that comprise a haplotype of *SMALL AUXIN*
271 *UP RNA 26* (*SAUR26***,** AT3G03850) (Fig. 3C). These variants were identified by GWA analysis using
272 a linear model (Fig. 3B; Table G3). To confirm that the identification of these candidates was not an
273 artifact due to population structure, we verified that these variants were also identified using two
274 different analyses that correct for population structure in the sample: an Accelerated Mixed Model
275 using GWAPP and an alternative Mixed Model approach, GWAS-Flow (these two SNPs are among
276 the green datapoints in Fig. S7A and C; see Table G3).

277 We additionally found from TWA analysis that the transcript levels of *SAUR26* are also
278 correlated with natural variation in leaf area plasticity in response to drought (Tables T1, T2).
279 eGWAS confirmed the cis-regulatory effect of the same two genetic variants as depicted in Fig. 3C
280 (cis-regulation; Fig. 3D; Table G6), consistent with the correlation between the genetic variation in
281 *SAUR26*, its transcript abundance, and leaf area plasticity.

282 Fig. 3E illustrates the haplotypic differences in leaf area plasticity for *SAUR26* in our study.
283 Accessions harboring the minor *SAUR26* haplotype display negative plasticity in rLA, while the
284 major *SAUR26* haplotype is associated with homeostatic and positive plasticity responses in rLA (Fig.
285 3E; Wilcoxon P-value < 0.001). These haplotypic differences were also associated with the transcript
286 levels of *SAUR26* (Fig. 3F), which we confirmed not only in the group of accessions included in our
287 study (Wilcoxon P-value < 0.001) but also in the much larger group of 189 Iberian accessions
288 included within the 1001 Genomes Project (Fig. 3F; Wilcoxon P-value < 0.001). Both the genetic
289 variation defined by this haplotype in *SAUR26* and the resulting *SAUR26* transcript abundance are
290 associated with the interplay between plasticity and homeostasis that we determine in our study (Figs
291 3E, F). These results highlight *SAUR26* as a candidate regulator of leaf area plasticity in response to
292 drought (Figs 3G, H).

293 In our GWA analysis on rLA (Fig. S8A, Table G1, G2), no SNPs were associated with rLA
294 under both well-watered and drought conditions, i.e., no SNPs were associated with homeostasis and
295 thus horizontal lines are absent from Fig. S8A. The results from TWA analysis were strikingly
296 different, identifying not only transcripts associated with leaf area plasticity but also transcripts
297 associated with leaf area homeostasis (Fig. 4; Fig. S8B). Regarding homeostasis, four transcripts are
298 positively correlated with rLA under both well-watered and drought conditions: *SOFL2*
299 *(AT1G68870), CPN60B (AT1G55490), AT5G39471, and CKL8 (AT5G43320)* (Fig. 4A). Accessions
300 with higher transcript abundance of these genes display a higher rLA under both well-watered and
301 drought conditions (Fig. 4B-E; note the similarity of the regression lines in each panel). Conversely,
302 we identified four genes negatively correlated with rLA: *RHF1A* (AT4G14220), *AT5G60160*,
303 *AT4G15260*, and *AT5G16800* (Fig. 4F). Accessions with a higher transcript abundance of these genes
304 display lower rLA under both well-watered and drought conditions (Fig. 4G-J; note the similarity of
305 the regression lines in each panel).
306

307 **Trade-off between plasticity and intrinsic water use efficiency**

308 It was not surprising to find a trade-off between growth and drought resistance among the accessions
309 in our study (Fig. 2D), as this is a well-established phenomenon (Zhang *et al.*, 2020). Accordingly,
310 we hypothesized that those accessions that displayed a homeostatic response to drought minimized
311 water loss, and thus would exhibit an increased intrinsic water-use efficiency (WUE_i). Given that
312 $\delta^{13}C$ reflects intrinsic water use efficiency (WUE_i) (Juenger *et al.*, 2005; Easlon *et al.*, 2014), we
313 analyzed the $\delta^{13}C$ values recorded by Dittberner *et al.* (2018), available for 21 of the accessions used
314 in our study. The results confirm a trade-off between plasticity and WUE_i (Fig. 5A). Accessions that
315 exhibit strong negative plasticity following drought (negative leaf area plasticity indices) have a lower
316 WUE_i in the absence of drought (more negative $\delta^{13}C$ values). Those accessions that maintain or
317 increase leaf area in response to drought (positive leaf area plasticity indices) display a higher WUE_i
318 in the absence of drought (more positive $\delta^{13}C$ values).
319 GWA analysis failed to identify any genetic variants associated with the observed phenotypic
320 trade-off between intrinsic WUE_i and leaf area plasticity (Fig. 5B; Table G3, G4), i.e., no datapoints
321 in the upper right quadrant of Fig. 5B. However, TWA analysis (Fig. 5C) provided insight into this
322 trade-off. Red datapoints in Fig. 5C are transcripts with greater abundance in those negatively plastic
323 and less water-use efficient accessions depicted in red in Fig. 5A; GO analysis revealed that these

were enriched in processes involved in RNA modification (Table GO2); we chose the putative pseudouridine synthase *CBF5* (*AT3G57150*) as an example (Figs 5D, E). Conversely, green points in Fig. 5C represent transcripts with greater abundance in the homeostatic and water-use efficient accessions depicted in green in Fig. 2D. We chose *CYCLIC NUCLEOTIDE-GATED CHANNEL 16* (*AT3G48010*; *CNGC16*) as an example (Figs 5F, G).

We determined that in our study, accessions that in response to drought displayed either increased or homeostatic leaf area plasticity also had higher WUE_i in the absence of drought (Fig. 5A). We then conducted a meta-analysis on the 95 Iberian accessions with published $\delta^{13}C$ information (Dittberner *et al.*, 2018). GWA analysis of these accessions rendered a distinctive peak in a single gene, identifying a haplotype consisting of eight co-varying SNPs in *ClpX3* (*AT1G33360*; Fig. 6A; Table G5), an ATP-dependent Clp protease subunit that plays essential roles in chloroplast development (Kim *et al*., 2009). Consistent with this result but more informative was the TWA analysis of WUE_i in the 88 Iberian accessions with both published transcript abundance and $\delta^{13}C$ information (Fig. 6B): we uncovered a distinctive enrichment in photosynthesis-related genes (Fig. 6C; Table GO3) among transcripts that are upregulated in accessions with high WUE_i (more positive $\delta^{13}C$ values; Fig. 6B; Table T1, T2). We highlight the positive relationships with WUE_i uncovered for the transcript abundance of *RuBisCO small subunit 2B* (*AT5G38420*; *RBCS2B;* Fig. 6D) and the positive relationship between the transcript abundance of *SAUR26* and WUE_i (Fig. 6E), in concordance with other findings in our study.

DISCUSSION

Identifying candidate regulators of plasticity and homeostasis

An adaptive trade-off between growth and drought resistance in plants is well-established (Zhang *et al.*, 2020). In productive environments, accessions with higher rLA in the absence of drought may have an advantage in competing for aboveground resources relative to smaller individuals, as proposed by Tilman (1988). On the other hand, plants adapted to unproductive environments typically fix less carbon, have higher WUE_i, and display reduced vegetative growth, even when grown in rich environments (Parsons, 1968; Chapin, 1991); however, these plants are typically stress-tolerant (Billings and Mooney, 1968; Grime, 1974, 1977). In our study, accessions typical of more productive areas display strong and negative plastic responses to drought (Fig. 3A). Conversely, accessions with

355 homeostatic or even positive plasticity in rLA in response to drought typify less productive areas (Fig.
356 3A). Here, we sought to identify the genetic basis of these contrasting ecological strategies.
357 Our main interest was not to identify natural variation associated with well-watered or drought
358 phenotypes, but rather natural variation associated with the degree of plasticity evoked in response to
359 drought, i.e., natural variation associated with reaction norms, rather than with phenotypes in one
360 environment or the other (well-watered or droughted). In exploring the genetic basis of plasticity, we
361 identified 31 genes corresponding to the top 50 candidate SNPs with the strongest association with
362 the leaf area plasticity index (Fig. 3B; Table 1; Table G3). To the best of our knowledge, 20 out of
363 these 31 genes have been previously characterized, and many of these are related to auxin regulation
364 and leaf expansion. This enrichment in auxin-related processes was confirmed by GO analysis (Table
365 GO1). Notably, when we compare the candidates resulting from GWA analysis on rLA vs. leaf area
366 plasticity, only eight candidate SNPs overlapped between both traits (green datapoints in Fig. S9A),
367 and none of these eight SNPs are in genes related to auxin. In other words, the auxin-related candidate
368 genes are related to *plasticity* in this trait and not to the trait itself.
369 The variant with the strongest association with the plastic response to drought was the auxin
370 efflux carrier family protein *PIN8* (*AT5G15100*). Among the associated SNPs, we also found two co-
371 varying SNPs in *AUXIN RESPONSE FACTOR 16* (*ARF16*; *AT4G30080),* two co-varying SNPs in
372 *SMALL AUXIN UP RNA 26* (*SAUR26*; *AT3G03850*); two variants in *AGAMOUS-like 15*
373 (*AT5G13790*; *AGL15*), a gene that negatively regulates auxin signaling in Arabidopsis (Zheng *et al.*,
374 2016); and three variants in *LONESOME HIGHWAY LIKE 1* (*LL2*; *AT2G31280*), an atypical basic
375 helix-loop-helix (bHLH) transcription factor that regulates early xylem development downstream of
376 auxin (Ohashi-Ito *et al.*, 2013).
377 Among the candidates that are not formally included in the GO category "response to auxin,"
378 we found six co-varying SNPs in the abscisic acid receptors *PYR1-like 11* (*PYL11*; *AT5G45860*) and
379 *PYR1-like 12* (*PYL12*; *AT5G45870*). ABA and auxin pathways interact in the regulation of growth
380 (Emenecker & Strader 2020), and also in the regulation of plasma membrane H^+ ATPases (of which
381 there is one member in the list, *H^+ ATPase 2* (*AHA2; AT4G30190*)) during cell expansion (Spartz *et*
382 *al.,* 2014) and stomatal control (Wong *et al*., 2021). We also found four co-varying SNPs in the *Basic*
383 *helix-loop-helix (bHLH) DNA-binding family protein MYC3* (*AT5G46760*), a known regulator of
384 glucosinolate biosynthesis (Schweizer *et al.*, 2013). Auxin negatively regulates glucosinolate levels,
385 which appears to integrate growth and stomatal regulation during drought (Salehin *et al.*, 2019) and

386 ABA response (Zhao *et al*., 2008). GO biological process analysis on positively correlated candidates
387 resulting from TWAS analysis on leaf area plasticity index for drought also revealed an enrichment
388 of glucosinolate biosynthesis genes (Table GO4).

389 We found that among the auxin-related variants associated with leaf area plasticity (Fig. 3B),
390 SNPs in *SAUR26* were of particular interest. The majority of characterized *SAUR* genes are positive
391 regulators of plant growth (Spartz *et al.*, 2014; Li *et al.*, 2015; Stortenbeker and Bemer, 2019).
392 Previous studies identified a regulatory role of *SAUR26* in rosette growth plasticity in response to
393 temperature changes (Wang *et al.*, 2019; Wang *et al.,* 2021). High temperatures accelerate
394 evaporative water loss from the plant while drought limits water availability, and these stresses
395 commonly co-occur. A reduction in leaf area is a common adaptive mechanism to maintain the
396 relative water content of plants under water deficit (Anyia and Herzog 2004). These previous studies
397 serve as validation of the role of *SAUR26* in regulating rosette plasticity to drought stress as
398 implicated by our study (Figure 2).

399 The two variants in *SAUR26* associated with rosette size were found in the 5' and 3' UTR,
400 respectively (Fig. 3C), regions of the transcript that typically regulate gene expression. Indeed, we
401 found the transcript levels of *SAUR26* to be associated with this genetic variation in *SAUR26* itself
402 (cis-regulation; Fig. 3D), which we confirmed both in the group of accessions included in this study
403 and, importantly, in the larger group of 189 Iberian accessions in the 1001 Genomes Project (Fig.
404 3F). The minor haplotype is associated with negative plasticity in leaf area in response to drought.
405 Conversely, the major haplotype, associated with higher transcript abundance of *SAUR26*, is
406 associated with leaf area homeostasis and positive plastic responses (Fig. 3E).

407 The location of these *SAUR26* variants in non-coding regions of the mRNA implicated
408 alteration in transcript abundance as a molecular phenomenon underlying the phenotypic correlations.
409 Indeed, natural variation in transcript abundance of *SAUR26* explained 18% of the observed plastic
410 response in leaf area to drought in our study (Fig. 3G, H). The importance of *SAUR26* transcript
411 abundance is supported by previous work that identified cis-elements in the 5' upstream region or the
412 3'UTR region of *SAUR26* that were associated with growth thermo-responsiveness of the rosette
413 compactness index (Wang *et al.*, 2019), (Wang *et al.* 2021), again validating our work. This
414 conclusion is also supported by our meta-analysis of the larger Iberian population with transcriptome
415 data, which also identified *SAUR26* transcript abundance as positively correlated with higher WUE_i
416 (Fig. 6B, E), along with other related auxin-related transcripts such as *AUXIN RESISTANT 3* (*AXR3*,

417 also known as *IAA17*, *AT1G04250;* Fig. S10A) (Leyser *et al.*, 1996) and *SMALL AUXIN*
418 *UPREGULATED 15* (*SAUR15*, *AT4G38850*; Fig. S10B) (Oh *et al.*, 2014). As we uncover in this
419 study, both transcript abundance and natural genetic variation in *SAUR26* cis-regulatory elements are
420 associated with the interplay between plasticity and homeostasis in rLA following drought stress (Fig.
421 3, Tables G3, T1, T2).

422 Interestingly, the minor haplotype frequency for this *SAUR26* haplotypic variant in our study
423 sample (minor haplotypic frequency, MHF = 38.09%) is similar to the frequencies we find in the 189
424 accessions within the Iberian population (MHF = 35.98%). However, the minor haplotype in the
425 Iberian population becomes the haplotype in higher frequency (64.14%) in the global 1001 Genomes
426 collection (The 1001 Genomes Consortium, 2016). It has been shown that Iberian Arabidopsis
427 populations locally adapted to drought conditions in this region out-perform accessions from wetter
428 areas of Northern Europe when both are exposed to drought (Exposito-Alonso *et al.*, 2019).
429 Following this, given that the major haplotype in our study is associated with homeostatic responses
430 to drought (Fig. 3E) and that its frequency becomes reduced outside the drought-prone Iberian region,
431 we can speculate that this *SAUR26* haplotypic variant is under selection in the Iberian population,
432 conferring an adaptive advantage to the water-limited conditions of the region.

433 We did not identify any SNPs associated with rLA under both well-watered and drought
434 conditions. Therefore, the genetic basis of growth homeostasis under drought could not be defined in
435 our study using GWAS (Fig. S8A). On the other hand, the reaction norms based on the strength of
436 association of transcript abundance with rLA, i.e., TWAS, identify four transcripts that are positively
437 correlated with rLA under both well-watered and drought conditions (Figs 4A-E, S8B). This means
438 that accessions with greater transcript abundance for those genes display higher rLA under both well-
439 watered and drought conditions. Conversely, we identified four transcripts negatively correlated with
440 rLA such that accessions with a higher transcript abundance of those genes display lower rLA under
441 both well-watered and drought conditions (Fig. 4F-J). Therefore, these eight genes are strong
442 functional candidates for the homeostatic regulation of rLA.

443 Of the eight resultant candidate genes, *CPN60B* (homeostatic, higher rLA) encodes a rubisco
444 large subunit-binding protein (Cheng *et al.*, 2020). *SOFL2* (homeostatic, higher rLA) is implicated in
445 the control of cytokinin content (Zhang *et al*., 2009), which can contribute to drought tolerance
446 (Rivero *et al.*, 2007), while *AT4G15260* (homeostatic, lower rLA) is a putative UDP-
447 glycosyltransferase, with another member of this superfamily identified as a cytokinin

448 glycosyltransferase (Hou *et al.*, 2004) that improves vegetative-stage drought survival when
449 overexpressed. *AT5G16800* encodes a N-terminal acetyl transferase for which null mutants exhibit
450 sensitivity to salinity stress. We can surmise functions in homeostatic control of leaf area for these
451 four genes based on their described functions and phenotypes. The other four homeostatic genes are
452 *AT5G39471* (annotated as a "Cysteine/Histidine-rich C1 domain family protein") and *CKL8*
453 (annotated as a casein kinase), both correlated with homeostatic and high rLAs, and *RHF1A* (RING-
454 finger E3 ubiquitin ligase (Liu *et al.*, 2008) and *AT5G60180* (vacuolar aminopeptidase (Park *et al.*,
455 2017), both correlated with homeostatic and low rLAs. For these genes further research is needed
456 regarding how they might contribute to homeostasis.
457

458 **Trade-off between relative leaf area (rLA), plasticity and WUE_i**

459 Plant species with low relative growth rates exhibit high WUE_i (Angert *et al.*, 2009; Kimball *et al.*,
460 2012). We can hypothesize that those plants with lower growth rates will have better drought
461 resistance, consequently displaying growth homeostasis. These observations are both consistent with
462 results from ecological studies and confirmed in crop species (Kasuga *et al.*, 1999; Ferrero-Serrano
463 and Assmann, 2016; Ferrero-Serrano *et al.*, 2018; Ferrero-Serrano et al., 2024). In our study,
464 accessions with lower rLA and homeostatic responses to drought display a greater abundance of
465 transcripts encoding functions related to ion transport (yellow datapoints in Fig. S9B; Tables T1, T2,
466 GO5), which could be related to osmoregulation and stomatal control of transpiration. Consistent
467 with this argument, the homeostatic response in rLA in response to prolonged drought that we observe
468 in our study correlates positively with a high predicted WUE_i recorded by Dittberner *et al.* (2018) for
469 the same accessions (Fig. 5A).

470 We then studied the genetic basis of this trade-off between rLA, plasticity, and WUE_i. There
471 were no SNPs associated with both the leaf area plasticity index and WUE_i (Fig. 5B). However, when
472 we compare the candidates obtained from TWA analysis, we identify transcripts associated with both
473 low WUE_i and a negative plastic response in leaf area following sustained drought (Fig. 5C).
474 Conversely, we also identify a set of transcripts that is significantly associated with both leaf area
475 homeostasis (more positive leaf area plasticity index) and increased WUE_i (Fig. 5C). To exemplify
476 these opposed responses to drought, given the enrichment in RNA modification and ion transport
477 genes that we found in the transcripts regulating the trade-off between relative leaf area and plasticity
478 (Fig S12B; Tables T1, T2), we highlight two of the genes identified by TWAS, with opposite

479 correlations between transcript abundance and relative leaf area plasticity (Figs 5D, E vs. Figs 5F,
480 G): (*CBF5*; *AT3G57150*) and *CYCLIC NUCLEOTIDE GATED CHANNEL 16* (*CNGC16*;
481 *AT3G48010*).

482 *CBF5* encodes a protein with homology to a category of pseudouridine synthases, and its
483 knockout in Arabidopsis is lethal (Lemontova *et al.,* 2007). Originally only non-coding RNAs,
484 particularly rRNAs, were thought to be pseudouridylated, but it is now recognized that mRNAs are
485 also a target for pseudouridylation. In both yeast and human cells, this post-transcriptional
486 modification is induced by heat shock, with consequent impacts on splicing, mRNA stability, and
487 translation (Karijolich *et al*., 2015), and some candidate pseudouridine synthases in rice have been
488 shown to be transcriptionally regulated by drought (Dingra et al., 2023). We observe that accessions
489 with higher transcript abundance of *CBF5* display both strong negative plastic responses in rLA in
490 response to drought (Fig. 5D) and reduced WUE_i (Fig. 5E). Our observations suggest that stress-
491 induced pseudouridylation may also occur in plants, with functional consequences for drought
492 tolerance; other types of mRNA modifications in plants have been correlated with increased mRNA
493 stability and translation under salinity stress (Kramer et al., 2020) and improved heat tolerance (Tang
494 *et al.,* 2020).

495 Conversely, transcript abundance of *CNGC16* is associated with homeostatic responses in
496 rLA and increased WUE_i. CNGCs are a superfamily of ion channels permeable to divalent and
497 monovalent cations (Köhler *et al.*, 1999; DeFalco *et al.*, 2016). *CNGC*s like *CNGC5* and *CNGC6*
498 have been reported to be the basis of a cyclic GMP (cGMP)-activated nonselective Ca^{2+}-permeable
499 cation channel activity in the plasma membrane of Arabidopsis guard cells (Wang *et al.*, 2013)
500 associated with stomatal closure. *CNGC16* is also critical for reproductive success following drought
501 stress (Tunc-Ozdemir *et al.*, 2013). Consistent with these functional roles, in our study, higher
502 transcript abundance of *CNGC16* is found in accessions with positive leaf area plasticity indexes
503 under drought (leaf area homeostasis; Fig. 5F); and with high WUE_i (Fig. 5G).

504 Given the increased plastic responses in leaf area found in accessions with lower WUE_i, we
505 next conducted a meta-analysis on the larger set of 95 Iberian accessions with $\delta^{13}C$ information from
506 a previous study focused on the global Arabidopsis population (Dittberner *et al.*, 2018). We identified
507 a distinctive peak consisting of eight co-varying SNPs in a single gene, *ClpX3* (*AT1G33360*; Fig.
508 6A), an ATP-dependent Clp protease subunit (Nishimura and van Wijk, 2015). Null mutants in a
509 different chloroplast protease subunit, ClpR, display a remarkable loss of chlorophyll (95 to 98%

510 reduction) and photosynthetic capacity, turning entirely white when grown under high light (Kim *et*
511 *al.*, 2009).

512 TWA analysis of WUE_i determined from $\delta^{13}C$ values in the 88 Iberian accessions with both
513 $\delta^{13}C$ information (Dittberner *et al.*, 2018) and published transcript abundance (Kawakatsu *et al.*,
514 2016) further supported the relationship with photosynthesis. Our TWAS on WUE_i in the larger
515 Iberian population identified 31 out of the 45 candidate genes for WUE_i that we also identified in the
516 subset of 20 Iberian accessions in our experimental study for which published $\delta^{13}C$ data were
517 available (Table T1 and T2). Gene Ontology (GO) biological process analysis of the resultant 45
518 candidates positively correlated with $\delta^{13}C$ uncovered an unequivocal enrichment in photosynthesis-
519 related genes for transcripts that are upregulated in accessions with high WUE_i (less negative $\delta^{13}C$
520 values; Figs 6B, 6C; Table GO3). Among the candidates from our TWA analysis that are positively
521 related to WUE_i was *RuBisCO small subunit 2B* (*AT5G38420*; *RBCS2B;* Figs 6B, D). An
522 upregulation in *RuBisCO* may compensate for suboptimal CO_2 concentrations at the sites of
523 carboxylation arising from reduced stomatal apertures in plants from drought-prone environments.
524 We illustrate eight additional genes with transcript abundances that were positively associated with
525 WUE_i in Fig. S10. Among these are *NADH dehydrogenase-like complex M* (*NdhM*, *AT4G37925;* Fig.
526 S10C), required for *NdH* complex assembly (Ifuku *et al.*, 2011), and *High cyclic electron flow 1*
527 (*HCEF1*; *AT3G54050*; Fig. S10D; Livingston *et al.*, 2010), both regulators of cyclic electron flow
528 around PSI (Yamori *et al.*, 2011), *ATP-Synthase δ-Subunit* (*ATPD*, *AT4G09650*; Fig. S10E)
529 (Maiwald *et al.*, 2003), *Photosystem I reaction center subunit PSI-N* (*PSAN*, *AT5G64040;* Fig. S10F)
530 (Haldrup *et al.*, 1999), and *Photosystem II subunit O-2* (*PSBO2*; *AT3G50820;* Fig. S10G) (Murakami
531 *et al.*, 2005). Also, the candidate with the highest association score is a member of the plasma
532 membrane intrinsic protein (PIP) subfamily of aquaporins (*PIP1;5*; *AT4G23400*; Fig. S10H). PIPs
533 regulate water flux in guard cells as well as membrane permeability to CO_2 in the mesophyll, with an
534 important effect on mesophyll conductance and CO_2 concentration at the sites of carboxylation (C_c)
535 (Groszmann *et al.*, 2017; Zait, Ferrero-Serrano & Assmann 2021). Thus, *PIP1;5* is also a candidate
536 regulator of photosynthetic rates. As discussed before, *SAUR26* is also among these candidates (Fig.
537 6B, E), increasing our confidence in the role of this gene as a regulator of plastic responses to drought
538 (Fig. 3).

539 Among the candidates that are negatively related to high WUE_i there is an enrichment in
540 carbohydrate transport-related processes (Table GO6). We can speculate that this enrichment reflects

541 the transport of carbohydrates produced during photosynthesis to promote plant growth. This would
542 be concordant with the trade-off between growth and WUE_i that we observe in our study.
543

544 ## Conclusions

545 The adaptive role of plasticity has been at the center of a long-standing debate. Much work and
546 discussion have focused on the principle that if plasticity is indeed adaptive, it may be under genetic
547 control (Bradshaw, 1965; Via *et al.*, 1995); however, few relevant genes have been identified. Here,
548 we propose that not only plasticity but also homeostasis is under genetic control and subject to natural
549 selection. This concept is supported by our dissection of the genetic basis of both plasticity and
550 homeostasis in leaf area following drought, which identifies specific genes implicated in each
551 process.

552 Knowledge from natural populations of how plants adapt to their environment can be
553 incorporated in breeding and biotechnological approaches to crop improvement. In this study, we
554 observe a trade-off between growth and drought response. A similar trade-off between stress
555 tolerance and productivity threatens food security. It is noteworthy that we also found accessions that
556 did not display this trade-off, e.g., those accessions marked in green in Fig. 2D, E. These accessions
557 may be of particular interest from an agronomic perspective.

558 While candidate genes other than *SAUR26* identified in our study await experimental
559 validation, their identification represents a significant step forward in understanding the genetic basis
560 and mechanisms of plasticity and homeostasis. In particular, the concerted use of TWAS and GWAS
561 increases the power to link genes to phenotypes (Kremling et al., 2019). A similarly integrative
562 approach has identified water use efficiency traits in sorghum (Ferguson *et al*., 2020). Here, this
563 approach has yielded insights into the genetic basis of response to resource limitation, identifying
564 both candidate "plasticity genes" and candidate "homeostasis genes" for further study. In particular,
565 the identification of potential homeostatic mechanisms has important implications for maintaining
566 crop yield in the face of climate change. Results arising from diverse genome-wide analyses in both
567 model and crop species (Schindele *et al*., 2020) can now be used to inform powerful new CRISPR-
568 based approaches for gene editing and modulation of transcript abundance toward crop improvement
569 (Abudayyeh *et al*., 2017).

570 ## Figures

571 **Fig. 1.** Conceptual framework for the adaptive role of plastic and homeostatic responses across
572 productivity gradients in the local environment. (A) Schematic illustration representing the balance
573 *sensu* Grime (1974, 1977), between stress tolerance in lower productivity, stress-prone environments,
574 and competitive ability in and homeostasis in plants. In less productive environments, homeostatic
575 responses to stress and lower relative growth rates result in lower biomass production, which is tuned
576 in to the lower resources that are typically available in their environment and favors adaptation to
577 those environments. In contrast, in productive environments, in which competition becomes more
578 intense, plastic responses are favored from an adaptive standpoint. (B). In unproductive
579 environments, frequent stress events can increase the allostatic load in individuals adapted to high-
580 productivity environments where plastic responses are beneficial. During the lifetime of an
581 individual, this results in a maladaptive response that increases allostatic load. In contrast, individuals
582 adapted to unproductive environments exhibit less plastic (more homeostatic) responses to repeated
583 stress that reduces their allostatic load over their lifetime.
584
585 **Fig. 2.** Accession-specific rosette leaf area responses in Arabidopsis. (A) Detail of the common
586 garden experiment, illustrating the randomization of well-watered and drought treatments, as
587 reflected in soil coloration. (B) Phenotypic reaction norms illustrating a reduction of leaf area in
588 response to drought in most but not all accessions. Violin distributions represent probability densities
589 of leaf area (cm^2) among the accessions included in this study. Datapoints depict the mean phenotypic
590 values of individual accessions, and the reaction norms represent the plastic response in the leaf area
591 of each accession in response to drought (t-test; P-value < 0.001). (C) Phenotypic reaction norms
592 illustrating plastic and homeostatic responses in relative leaf area (rLA). Violin distributions represent
593 probability densities of rLA among the accessions included in this study. Datapoints depict the rLA
594 of individual accessions, and the reaction norms represent the plastic response in rLA of each
595 accession in response to drought (t-test; P-value > 0.05). (D) Negative relationship (P-value < 0.05)
596 between leaf area plasticity index (slope of the reaction norms in 2C) in response to drought (y-axis)
597 and rLA under well-watered conditions (x-axis). Data were fitted using a linear regression model.
598 Grey shadow represents the 95% CI of the fit regression line. Four different quadrants are defined by
599 two dashed lines: the average rLA (x-axis), and y = 0, which is the homeostatic point at which a
600 change in water availability does not affect rLA (i.e. a plasticity index of 0). Data points depict

601 individual accessions with their respective label. Data points are colored based on in which quadrant
602 they fall (see text). (E) Images illustrating the plastic and homeostatic responses to drought found
603 among the accessions included in this study.

604 **Fig. 3.** *SMALL AUXIN UP RNA 26* (*SAUR26***,** AT3G03850**)** is a candidate regulator of Arabidopsis
605 leaf area plasticity in response to drought. (A) Accessions from more productive areas display
606 stronger negative reductions in leaf area plasticity relative to accessions from less productive
607 environments. Scatter plot depicting the negative relationship (P-value < 0.05) between leaf area
608 plasticity index (y-axis) and Net Primary Productivity during the spring season (x-axis). (B)
609 Manhattan plot representing the strength of association between genetic variants and leaf area
610 plasticity in response to drought. (C) *SAUR26* gene model, including the two co-varying SNPs
611 highlighted in 2B. Orange block depicts the sole exon, green block the 5' UTR, dark green block the
612 3' UTR. Labels above indicate the position of the two SNPs that co-vary, forming a haplotype in our
613 sample. Major/minor allele frequency in our sample, in the 189 accessions from the Iberian Peninsula
614 included in the 1001 Genome Project, and the whole 1001 Genomes Project sample dataset is
615 provided. (D) Manhattan plot representing the genome-wide strength of association between the
616 genetic variation present within the 665 accessions from the transcript abundance reference panel
617 (Kawakatsu *et al.*, 2016) that overlap with the collection of accessions included in the 1001 Genomes
618 Project, and the variation in the transcript abundance of *SAUR26* (Kawakatsu *et al.*, 2016). The peak
619 in chromosome 3 represents the cis-genetic variants in *SAUR26* affecting its transcript abundance.
620 For the Manhattan plots in 3B and D, the score (y-axis) consists of the negative logarithm of the P-
621 value and provides association strength. Each data point represents a SNP with a color corresponding
622 to the chromosome where the genetic variants are located. The x-axis and the different colors shown
623 in the SNPs depicted in the Manhattan plots represent the different chromosomes. The higher the
624 score, the lower the P-value, and the stronger the association between genetic variation and leaf area
625 plasticity or *SAUR26* transcript abundance. (E) In the Iberian population, the major haplotype of
626 *SAUR26* is associated with homeostatic or positive responses of relative leaf area (rLA) in response
627 to drought. Conversely, the minor haplotype in the Iberian population is associated with plastic
628 responses in rLA in response to drought. Violin plots show significantly different probability
629 densities of leaf area plasticity in response to drought for the major and minor allele haplotypes in
630 *SAUR26.* (F) The haplotypes in *SAUR26* associated with leaf area plasticity/homeostasis in response
631 to drought are associated with differences in *SAUR26* gene expression. Violin plots show significantly

632 different probability densities of *SAUR26* transcript abundance for the major and minor allele
633 haplotypes in *SAUR26* for both our sample and the entire Iberian population. (G) Scatter plot
634 illustrating the positive relationship between leaf area plasticity index (y-axis) and *SAUR26* transcript
635 abundance (x-axis). For 2A and 2G, the grey shadow represents the 95% CI of the fit regression line
636 (dark grey). (H) Cartoon illustrating the regulatory role of genetic and transcript variation in *SAUR26*
637 and the response of leaf area to drought.

638 **Fig. 4.** Transcriptomic reaction norms uncover genetic correlates of Arabidopsis leaf area
639 homeostasis in response to drought. (A) homeostatic reaction norms for transcripts significantly and
640 positively correlated with relative leaf area (rLA) under both watering regimes. (B) to (E). Scatter
641 plots illustrating positive and homeostatic relationships (*P*-value < 0.05) between rLA under both
642 well-watered (closed circles) and drought conditions (open circles) conditions (y-axis), and transcript
643 abundance (FPKM; x-axis) of (B) AT5G39471, (C) *SOB FIVE-LIKE 2* (*SOFL2; AT1G68870*)**,** (D)
644 *CHAPERONIN 60 BETA* (*CPN60B*; *AT1G55490*), and (E) *CASEIN KINASE I-LIKE 8* (*CKL8*;
645 *AT5G43320*). (F) homeostatic reaction norms for transcripts significantly and negatively correlated
646 with rLA under both watering regimes. (G) to (J) Scatter plots illustrating negative and homeostatic
647 relationships (*P*-value < 0.05) between rLA under both well-watered (closed circles) and drought
648 conditions (open circles) (y-axis), and transcript abundance (FPKM; x-axis) of (G) AT5G60160, (H)
649 *AT4G15260***,** (I) *AT5G16800*, and (J) *RING-H2 GROUP F1A* (*RHF1A*; *AT4G14220*). For 3a and 3f,
650 Spearman's rank correlation coefficient ($r_{s;}$ y-axis) indicates the correlation between the rLA and the
651 natural variation in transcript abundance of each gene. In Figs B to E and G to J, data were fitted
652 using a linear regression model. Also, in panels b-e and g-j, filled circles depict the rLA of accessions
653 grown under well-watered conditions, while empty circles squares depict the rLA of accessions
654 grown under drought.
655

656 **Fig. 5.** Arabidopsis accessions that display leaf area homeostasis in response to drought, display
657 higher water use efficiency as defined by $\delta^{13}C$. **(**A**)** Scatter plot illustrating the positive relationship
658 (*P*-value < 0.05) between leaf area homeostasis in response to drought (leaf area plasticity index, y-
659 axis) and water use efficiency (x-axis) among Iberian Arabidopsis accessions used in this study. Data
660 were fitted to a linear regression model. Grey shadow represents the 95% CI of the fit regression line
661 (black). $\delta^{13}C$ data for the accessions were retrieved from Dittberner *et al.* (2018). Four different

662 quadrants are defined by two dashed lines: y = 0, which is the homeostatic point at which a change
663 in water availability does not affect relative leaf area (i.e., a plasticity index of 0), and the average
664 intrinsic water use efficiency (WUE_i, $\delta^{13}C$; x-axis). Data points depict individual accessions with
665 their respective labels. **(**B) The genetic basis of leaf area plasticity in response to drought and water
666 use efficiency. This plot depicts the respective relationship between the GWAS associations found
667 for the leaf area plasticity index in response to drought (y-axis) and those for WUE_i (Dittberner *et al.*,
668 2018) (x-axis). Data points represent individual SNPs. The y-axis and x-axis depict the extent of the
669 association with, respectively, leaf area plasticity, and WUE_i, as the negative logarithm of the p-value.
670 Dashed lines depict an arbitrary threshold for significance that is consistent across comparisons. (C)
671 Transcriptomic association with plastic leaf area responses to drought and WUE_i. Spearman's rank
672 correlation depicts the relationship between the association of the transcript abundance of each gene
673 in the Arabidopsis genome with leaf area plasticity in response to drought (r_s) on the y-axis and with
674 WUE_i on the x-axis. Dashed lines define an arbitrary threshold to consider transcripts correlated
675 positively ($r_s \geq 0.4$) or negatively ($r_s \leq -0.4$) associated with leaf area plasticity (y-axis) or WUE_i (x-
676 axis). *CBF5* and *CNGC16* exemplify transcripts with opposing relationships to leaf area plasticity
677 and water use efficiency as shown in 4C, D and E. Scatter plots depicting the relationship (P-value <
678 0.05) between leaf area plasticity index in response to drought (4D), or water use efficiency (4E) on
679 the y-axis, and transcript abundance (FPKM) of *CBF5* on the x-axis. F and G. Scatter plots depicting
680 the relationship (*P*-value < 0.05) between (4F) leaf area plasticity index in response to drought or
681 (4G) water use efficiency (Dittberner *et al.*, 2018) on the y-axis, and transcript abundance (FPKM)
682 of *CYCLIC NUCLEOTIDE-GATED CHANNEL 16* (*CNGC16*) on the x-axis. In all panels, data were
683 fitted using a linear regression model. Grey shadow represents the 95% CI of the fit regression line.

684

685 **Fig. 6.** Photosynthesis-related transcript variants regulate water use efficiency in Iberian Arabidopsis
686 accessions**. (**A) Manhattan plot representing the genome-wide strength of association between genetic
687 variation and variation in $\delta^{13}C$ present within 95 Iberian accessions with $\delta^{13}C$ values available from
688 Dittberner *et al*. (2018). The score (y-axis) consists of the negative logarithm of the *P*-value and
689 provides association strength. Inset: Violin plots representing the probability densities of WUE_i for
690 the major and minor allele haplotypes in *ClpX* for the accessions included in Fig. 6A. (B) T-
691 Manhattan plot representing transcriptome-wide strength of association between variation in
692 transcript abundance (Kawakatsu *et al.*, 2016) and natural variation in $\delta^{13}C$. This analysis was

693 performed on all Iberian accessions with both transcript abundance data (Kawakatsu *et al.*, 2016) and
694 $\delta^{13}C$ information (Dittberner *et al.*, 2018) (n = 88 accessions). The relationship is defined by the
695 Spearman's rank correlation coefficient (r_s). Dashed lines define an arbitrary threshold for positive
696 ($r_s \geq 0.4$) or negative ($r_s \leq -0.4$) correlation with water-use efficiency (y-axis). Blue labels highlight
697 the transcripts positively associated with higher WUE_i, while red labels highlight those negatively
698 associated with higher WUE_i. (C) Hierarchical clustering tree summarizing the correlation among
699 significant GO Biological Process categories resulting from analysis of the positively correlated
700 candidates resulting from TWA analysis of water use efficiency determined from $\delta^{13}C$ values in 88
701 Iberian Arabidopsis accessions. Ratios provide the number of genes positively correlated with WUE_i
702 within each GO category relative to the total number of genes within that category. The size of the
703 blue dots increases proportionally with P-value significance. (D) Scatter plot depicting the positive
704 relationship (*P*-value < 0.05) between WUE_i (y-axis) and *RuBisCO SMALL SUBUNIT 2B*
705 (*AT5G38420*; *RBCS2B*) transcript abundance (x-axis) for the Iberian accessions included in Fig. 6B.
706 **(**E**)** Scatter plot depicting the positive relationship (*P*-value < 0.05) between intrinsic water-use
707 efficiency (WUE_i; y-axis) and *SMALL AUXIN UP RNA 26* (*SAUR26,* AT3G03850) transcript
708 abundance (x-axis) for the Iberian accessions included in 6b. Inset: Scatter plot depicting the positive
709 relationship (*P*-value < 0.05) between intrinsic water-use efficiency (WUE_i; y-axis) and *SMALL*
710 *AUXIN UP RNA 26* (*SAUR26,* AT3G03850) transcript abundance (x-axis) for the 43 accessions
711 included in our study. For 5D, and 5E, gray shadow represents the 95% CI of the fit regression line
712 (black).

713 # Tables

714 **Table 1.** List of 31 genes corresponding to the top 50 candidate SNPs with the strongest association
715 with the leaf area plasticity index. Genes encoding proteins with auxin-related functions from GO
716 analysis are bolded; additional genes related to auxin based on literature analysis are underlined.

Chr	Position	MAF (%)	Gene ID	Gene description	Label
5	**4892996**	**38.24**	***AT5G15100***	***Auxin efflux carrier family protein***	***PIN8***
3	1787622	26.47	*AT3G05970*	*long-chain acyl-CoA synthetase 6*	*LACS6*
4	**14703801**	**26.47**	***AT4G30080***	***auxin response factor 16***	***ARF16***
4	**14705049**	**26.47**	***AT4G30080***	***auxin response factor 16***	***ARF16***
5	5238732	23.53	*AT5G16030*	*mental retardation GTPase activating protein*	*AT5G16030*
3	975320	32.35	*AT3G03810*	*O-fucosyltransferase family protein*	*EDA30*
3	970856	20.59	*AT3G03800*	*syntaxin of plants 131*	*SYP131*
5	15293597	26.47	*AT5G38280*	*PR5-like receptor kinase*	*PR5K*
5	15293610	26.47	*AT5G38280*	*PR5-like receptor kinase*	*PR5K*
5	15293481	41.18	*AT5G38280*	*PR5-like receptor kinase*	*PR5K*

4	14691629	35.29	*AT4G30060*	*Core-2/I-branching beta-1,6-N-acetylglucosaminyltransferase family protein*	*AT4G30060*
5	4659907	35.29	*AT5G14450*	*GDSL-like Lipase/Acylhydrolase superfamily protein*	*AT5G14450*
5	18974632	20.59	*AT5G46760*	*Basic helix-loop-helix (bHLH) DNA-binding family protein*	*MYC3*
5	18974915	20.59	*AT5G46760*	*Basic helix-loop-helix (bHLH) DNA-binding family protein*	*MYC3*
5	18975625	20.59	*AT5G46760*	*Basic helix-loop-helix (bHLH) DNA-binding family protein*	*MYC3*
5	18975826	20.59	*AT5G46760*	*Basic helix-loop-helix (bHLH) DNA-binding family protein*	*MYC3*
3	**983189**	**38.24**	***AT3G03850***	***SAUR-like auxin-responsive protein family***	***SAUR26***
3	**983517**	**38.24**	***AT3G03850***	***SAUR-like auxin-responsive protein family***	***SAUR26***
3	1798927	29.41	*AT3G05990*	*Leucine-rich repeat (LRR) family protein*	*AT3G05990*
5	4433730	29.41	*AT5G13740*	*zinc induced facilitator 1*	*ZIF1*
5	4433740	29.41	*AT5G13740*	*zinc induced facilitator 1*	*ZIF1*
5	4436472	29.41	*AT5G13740*	*zinc induced facilitator 1*	*ZIF1*
5	4436745	29.41	*AT5G13740*	*zinc induced facilitator 1*	*ZIF1*
5	4442005	29.41	*AT5G13760*	*Plasma-membrane choline transporter family protein*	*AT5G13760*
5	**4450177**	**29.41**	***AT5G13790***	***AGAMOUS-like 15***	***AGL15***
5	**4450180**	**29.41**	***AT5G13790***	***AGAMOUS-like 15***	***AGL15***
2	13323264	23.53	*AT2G31260*	*autophagy 9*	*APG9*
2	13330862	23.53	*AT2G31270*	*CDT1-like protein A*	*CDT1A*
2	13341047	23.53	*AT2G31280*	*transcription factor bHLH155-like protein*	*LL2*
2	13341186	23.53	*AT2G31280*	*transcription factor bHLH155-like protein*	*LL2*
2	13342866	23.53	*AT2G31280*	*transcription factor bHLH155-like protein*	*LL2*
2	13343940	23.53	*AT2G31290*	*Ubiquitin carboxyl-terminal hydrolase family protein*	*AT2G31290*
2	13345229	23.53	*AT2G31290*	*Ubiquitin carboxyl-terminal hydrolase family protein*	*AT2G31290*
2	13345701	23.53	*AT2G31290*	*Ubiquitin carboxyl-terminal hydrolase family protein*	*AT2G31290*
2	13346191	23.53	*AT2G31300*	*actin-related protein C1B*	*ARPC1B*
2	13358923	23.53	*AT2G31320*	*poly(ADP-ribose) polymerase 2*	*PARP1*
3	22329843	23.53	*AT3G60400*	*Mitochondrial transcription termination factor family protein*	*SHOT1*
4	14775183	32.35	*AT4G30190*	*H[+]-ATPase 2*	*AHA2*
4	6154596	32.35	*AT4G09770*	*TRAF-like family protein*	*AT4G09770*
1	29310771	20.59	*AT1G77960*	*repressor ROX1-like protein*	*AT1G77960*
5	18596240	20.59	*AT5G45840*	*Leucine-rich repeat protein kinase family protein*	*AT5G45840*
5	18604234	20.59	*AT5G45860*	*PYR1-like 11*	*PYL11*
5	18606400	20.59	*AT5G45870*	*PYR1-like 12*	*PYL12*
5	18606524	20.59	*AT5G45870*	*PYR1-like 12*	*PYL12*
5	18606721	20.59	*AT5G45870*	*PYR1-like 12*	*PYL12*
5	18606940	20.59	*AT5G45870*	*PYR1-like 12*	*PYL12*
5	18606953	20.59	*AT5G45870*	*PYR1-like 12*	*PYL12*
5	**18613579**	**20.59**	***AT5G45890***	***senescence-associated gene 12***	***SAG12***
5	3708088	20.59	*AT5G11550*	*ARM repeat superfamily protein*	*AT5G11550*
5	4655788	20.59	*AT5G14430*	*S-adenosyl-L-methionine-dependent methyltransferases superfamily protein*	*AT5G14430*

Supporting information

The following supplemental materials are available:

Fig. S1. Rosette leaf area observations at the time of flowering (Table P1).

Fig. S2. Quantile-quantile (QQ) plots for GWAS analysis using the Linear Model.

Fig. S3. Quantile-quantile (QQ) plots for GWAS analysis using the Accelerated Mixed Model.

Fig. S4. Quantile-quantile (QQ) plots for GWAS analysis using GWAS-Flow.

726 **Fig. S5.** Histograms of the distribution of r_s and scores obtained from GWA and TWA analyses of
727 the traits discussed in this study illustrate the stringent significance thresholds imposed in this study
728 (vertical dashed lines).
729 **Fig. S6.** The plasticity index that we calculated is predictive of the percentage change in leaf area
730 under drought relative to well-watered conditions.
731 **Fig. S7.** The identification of our candidate genes upon application of several different GWAS
732 methods improves confidence in candidates for leaf area plasticity and intrinsic water use efficiency
733 (WUE_i).
734 **Fig. S8.** Genotypic and transcriptomic reaction norms based on the strength of association of
735 individual SNPs and transcripts highlight the variation in the strength of these associations depending
736 on water availability.
737 **Fig. S9.** The genetic and transcriptomic basis of the relationship between leaf area plasticity potential
738 in response to drought with (Figs S9A, B) leaf area potential and (Figs S9C, D) intrinsic water use
739 efficiency (WUE_i).
740 **Fig. S10.** Illustration of candidate transcript variants that regulate intrinsic water use efficiency in
741 Iberian Arabidopsis accessions.
742 **Table P1.** Leaf area measurements recorded in this experiment (well-watered and drought).
743 Calculated relative leaf area (rLA) and plasticity, water use efficiency (WUE_i, $\delta^{13}C$) values recorded
744 by Dittberner *et al.* (2018) and MOD17A2 (net primary productivity) information obtained from
745 AraCLIM (Ferrero-Serrano & Assmann, 2019) for the accessions included in our study.
746 **Table P2.** Water use efficiency (WUE_i, $\delta^{13}C$) values recorded by Dittberner *et al.* (2018) for 95
747 Iberian Arabidopsis accessions.
748 **Table G1.** Candidates obtained from GWAS on relative leaf area (rLA) under well-watered
749 conditions. Only associations with a score ≥ 4 are included here. For a raw, unfiltered, as well as for
750 a fully filtered and annotated (see Materials & Methods) version of this GWAS output, please visit
751 the data repository.
752 **Table G2.** Candidates obtained from GWAS on relative leaf area (rLA) under drought. Only
753 associations with a score ≥ 4 are included here. For a raw, unfiltered, as well as for a fully filtered
754 and annotated (see Materials & Methods) version of this GWAS output, please visit the data
755 repository.

756 **Table G3.** Candidates obtained from GWAS on leaf area plasticity. Only associations with a score ≥
757 4 are included here. For a raw, unfiltered, as well as for a fully filtered and annotated (see Materials
758 & Methods) version of this GWAS output, please visit the data repository.
759 **Table G4.** Candidates obtained from GWAS on water use efficiency (WUE_i, δ13C) values recorded
760 by Dittberner *et al.* (2018) for the accessions included in our study. Only associations with a score ≥
761 4 are included here. For a raw, unfiltered, as well as for a fully filtered and annotated (see Materials
762 & Methods) version of this GWAS output, please visit the data repository.
763 **Table G5**. Candidates obtained from GWAS on water use efficiency (WUE_i, δ13C) values recorded
764 by Dittberner *et al.* (2018) for 95 Iberian Arabidopsis accessions. Only associations with a score ≥ 4
765 are included here. For a raw, unfiltered, as well as for a fully filtered and annotated (see Materials &
766 Methods) version of this GWAS output, please visit the data repository.
767 **Table G6.** Candidates obtained from eGWAS on the natural variation in transcript abundance of
768 *SAUR26* extracted from Kawakatsu *et al.* (2016). For a raw, unfiltered, as well as for a fully filtered
769 and annotated (see Materials & Methods) version of this GWAS output, please visit the data
770 repository.
771 **Table T1**. Results from TWAS (r_s).
772 **Table T2.** Results from TWAS (*P*-value).
773 **Table GO1.** GO analysis on the 31 genes corresponding to the top 50 candidate SNPs resulting from
774 GWAS analysis on leaf area plasticity index for drought.
775 **Table GO2.** GO analysis on the 58 genes identified from TWAS to exhibit transcript abundances
776 that are negatively correlated with leaf area plasticity index for drought, and negatively correlated
777 with water use efficiency determined from ($\delta^{13}C$) values from accessions overlapping with our sample
778 (red datapoints in Fig. 5C).
779 **Table GO3.** GO analysis on the 45 genes identified from TWAS to exhibit transcript abundances
780 that are positively correlated with water use efficiency determined from ($\delta^{13}C$) values in 88 Iberian
781 Arabidopsis accessions (datapoints with $r_s \geq 0.4$ in Fig. 6B).
782 **Table GO4.** GO analysis on the 494 genes identified from TWAS to exhibit transcript abundances
783 that are positively correlated with leaf area plasticity index for drought (green and grey datapoints
784 with $r_s \geq 0.4$ in the y-axis representing leaf area plasticity index in Fig. 5C).

785 **Table GO5.** GO analysis on the 28 genes identified from TWAS to exhibit transcript abundances
786 that are negatively correlated with relative leaf area (rLA) under well-watered conditions, and
787 positively correlated with leaf area plasticity index for drought (blue datapoints in S9B).
788 **Table GO6.** GO analysis on the 11 genes identified from TWAS to exhibit transcript abundances
789 that are negatively correlated with water use efficiency determined from ($\delta^{13}C$) values in 88 Iberian
790 Arabidopsis accessions (datapoints with $r_s \leq -0.4$ in Figure 6B).
791 **Table GO7.** GO analysis on the 302 genes identified from TWAS to exhibit transcript abundances
792 that are positively correlated with relative leaf area (rLA) under drought.
793 **Table GO8.** GO analysis on the 134 genes identified from TWAS to exhibit transcript abundances
794 that are negatively correlated with relative leaf area (rLA) under well-watered conditions (blue and
795 grey datapoints with $r_s \leq 0.4$ in the x-axis of Figure S9B).
796 **Table GO9**. GO analysis on the 177 genes identified from TWAS to exhibit transcript abundances
797 that are positively correlated with relative leaf area (rLA) under well-watered conditions (yellow and
798 grey datapoints with $r_s \geq 0.4$ in the x-axis of Figures S9B).
799 **Table GO10.** GO analysis on the 233 genes identified from TWAS that exhibit transcript abundances
800 which are negatively correlated with relative leaf area (rLA) under drought.
801

Acknowledgements

This research was supported by funding from The Pennsylvania State University to S.M.A. We thank Mr. Leland Burghard, Ms. Sarah Cronk, and Dr. Yotam Zait for greenhouse assistance. We thank Drs. David Chakravorty and Yotam Zait for helpful comments on the manuscript.

Author contributions

S.M.A & A.F-S. conceived the project, research plans, and experimental design. A.F-S. performed the experiments while S.M.A provided guidance throughout the experimental work. A.F-S. analyzed the data and prepared the figures; S.M.A supervised data analysis and figure preparation. S.M.A & A.F-S wrote the manuscript.

Data Availability

The data supporting the results are available as Supporting Information files. The code and data to easily reproduce the analysis, figures, and tables in this manuscript are available at https://github.com/AssmannLab and will be uploaded to Zenodo upon acceptance.

References

Abudayyeh OO, Gootenberg JS, Essletzbichler P, Han S, Joung J, Belanto JJ, Verdine V, Cox DBT, Kellner MJ, Regev A, *et al.* 2017. RNA targeting with CRISPR-Cas13. Nature **550**, 280–284.

Angert AL, Huxman TE, Chesson P, Venable DL. 2009. Functional tradeoffs determine species coexistence via the storage effect. Proceedings of the National Academy of Sciences, U.S.A. **106**, 11641–11645.

Anyia, AO, Herzog H. 2004. Water-use efficiency, leaf area and leaf gas exchange of cowpeas under mid-season drought. European Journal of Agronomy **20**, 327-339.

Billings WD, Mooney HA. 1968. The ecology of arctic and alpine plants. Biological Reviews **43**, 481–529

Bradshaw AD. 1965. Evolutionary significance of phenotypic plasticity in plants. Elsevier, pp 115–155.

830 **Castilla AR, Méndez-Vigo B, Marcer A, Martínez-Minaya J, Conesa D, Picó FX, Alonso-Blanco**
831 **C.** 2020. Ecological, genetic and evolutionary drivers of regional genetic differentiation in
832 *Arabidopsis thaliana*. BMC Evolutionary Biology **20**, 1-13.
833 **Chapin, FS.** 1991. Integrated responses of plants to stress. Bioscience **41**, 29–36.
834 **Cheng, CY, Krishnakumar, V, Chan, AP, Thibaud-Nissen, F, Schobel, S, & Town, CD.** 2017.
835 Araport11: a complete reannotation of the *Arabidopsis thaliana* reference genome. The Plant
836 Journal **89**, 789-804.
837 **Cheng X, Fang T, Zhao E, Zheng B, Huang B, An Y, Zhou P.** 2020. Protective roles of salicylic
838 acid in maintaining integrity and functions of photosynthetic photosystems for alfalfa
839 (*Medicago sativa L.*) tolerance to aluminum toxicity. Plant Physiology and Biochemistry **155**
840 570-578.
841 **Cingolani P, Platts A, Wang LL, Coon M, Nguyen T, Wang L, Land SJ, Lu X, Ruden DM.**
842 2012. A program for annotating and predicting the effects of single nucleotide
843 polymorphisms, SnpEff: SNPs in the genome of *Drosophila melanogaster* strain w1118; iso-
844 2; iso-3. Fly (Austin) **6**, 80–92.
845 **Coll JR, Aguilar E, Ashcroft L.** 2016. Drought variability and change across the Iberian Peninsula.
846 Theoretical and Applied Climatology **130**, 901-916.
847 **Condon AG, Richards RA, Rebetzke GJ, Farquhar GD.** 2002. Improving intrinsic water-use
848 efficiency and crop yield. Crop Science **42**, 122–131.
849 **DeFalco TA, Moeder W, Yoshioka K.** 2016. Opening the gates: insights into cyclic nucleotide-
850 gated channel-mediated signaling. Trends in Plant Science **21**, 903–906.
851 **Des Marais DL, McKay JK, Richards JH, Sen S, Wayne T, Juenger TE.** 2012. Physiological
852 genomics of response to soil drying in diverse Arabidopsis accessions. Plant Cell **24**, 893–
853 914.
854 **Dhingra Y, Lahiri M, Bhandari N, Kaur I, Gupta S, Agarwal M, Katiyar-Agarwal S.** 2023.
855 Genome-wide identification, characterization, and expression analysis unveil the roles of
856 pseudouridine synthase (PUS) family proteins in rice development and stress
857 response. Physiology and Molecular Biology of Plants **29**, 1981-2004.
858 **Dittberner H, Korte A, Mettler-Altmann T, Weber APM, Monroe G, de Meaux J.** 2018. Natural
859 variation in stomata size contributes to the local adaptation of water-use efficiency in
860 *Arabidopsis thaliana*. Molecular Ecology **27**, 4052–4065.

861 **Donat MG, Lowry AL, Alexander LV, O'Gorman PA, Maher N.** 2016. More extreme
862 precipitation in the world's dry and wet regions. Nature Climate Change **6**, 508–513.
863 **Dorn LA, Pyle EH, Schmitt J.** 2000. Plasticity to light cues and resources in *Arabidopsis thaliana*:
864 testing for adaptive value and costs. Evolution **54**, 1982–1994.
865 **Easlon HM, Nemali KS, Richards JH, Hanson DT, Juenger TE, McKay JK.** 2014. The
866 physiological basis for genetic variation in water use efficiency and carbon isotope
867 composition in *Arabidopsis thaliana*. Photosynthesis Research **119**, 119–129.
868 **Emenecker, R. J., & Strader, L. C.** 2020. Auxin-abscisic acid interactions in plant growth and
869 development. Biomolecules **10**, 281.
870 **Exposito-Alonso M, 500 Genomes Field Experiment Team, Burbano HA, Bossdorf O, Nielsen**
871 **R, Weigel D.** 2019. Natural selection on the *Arabidopsis thaliana* genome in present and
872 future climates. *Nature* **573**, 126–129.
873 **Exposito-Alonso M, Brennan AC, Alonso-Blanco C, Picó FX.** 2018a. Spatio-temporal variation in
874 fitness responses to contrasting environments in *Arabidopsis thaliana*. Evolution **72**, 1570-
875 1586.
876 **Exposito-Alonso M, Vasseur F, Ding W, Wang G, Burbano HA, Weigel D.** 2018b. Genomic basis
877 and evolutionary potential for extreme drought adaptation in *Arabidopsis thaliana*. Nature
878 Ecology & Evolution **2**, 352–358.
879 **Ferguson JN, Fernandes SB, Monier B, Miller ND, Allan D, Dmitrieva A, Schmuker P, Lozano**
880 **R, Valluru R, Buckler ES, *et al.*** 2020. Machine learning enabled phenotyping for GWAS
881 and TWAS of WUE traits in 869 field-grown sorghum accessions. Plant Physiology
882 10.1093/plphys/kiab346.
883 **Ferrero-Serrano Á, Assmann SM.** 2019. Phenotypic and genome-wide association with the local
884 environment of Arabidopsis. Nature Ecology & Evolution **3**, 274–285.
885 **Ferrero-Serrano Á, Assmann SM.** 2016. The α-subunit of the rice heterotrimeric G protein, RGA1,
886 regulates drought tolerance during the vegetative phase in the dwarf rice mutant *d1*. Journal
887 of Experimental Botany **67**, 3433–3443.
888 **Ferrero-Serrano Á, Cantos C, Assmann SM.** 2019. The role of dwarfing traits in historical and
889 modern agriculture with a focus on rice. Cold Spring Harbor Perspectives in Biology, **11**,
890 p.a034645.
891 **Ferrero-Serrano Á, Chakravorty D, Kirven KJ, Assmann SM.** 2024. Oryza CLIMtools: A

892 genome–environment association resource reveals adaptive roles for heterotrimeric G
893 proteins in the regulation of rice agronomic traits. Plant Communications. 100813.
894 **Ferrero-Serrano, Á, Chakravorty D.** 2023. Plants and heterotrimeric G proteins: Expect the
895 unexpected. Molecular plant, ***16*****,** 506-508.
896 **Ferrero-Serrano Á, Sylvia MM, Forstmeier, PC, Olson, AJ, Ware, D, Bevilacqua, PC,**
897 **Assmann, SM.** 2022. Experimental demonstration and pan-structurome prediction of
898 climate-associated riboSNitches in Arabidopsis. Genome biology, **23**, 101.
899 **Ferrero-Serrano Á, Su Z, Assmann SM.** 2018. Illuminating the role of the Gα heterotrimeric G
900 protein subunit, *RGA1*, in regulating photoprotection and photoavoidance in rice. Plant, Cell
901 & Environment **41**, 451–468.
902 **Forsman A.** 2015. Rethinking phenotypic plasticity and its consequences for individuals, populations
903 and species. Heredity **115**, 276–284.
904 **Frachon L, Bartoli C, Carrère S, Bouchez O, Chaubet A, Gautier M, Roby D, Roux F.** 2018. A
905 genomic map of climate adaptation in *Arabidopsis thaliana* at a micro-geographic scale.
906 Frontiers in Plant Sciences **9**, 967.
907 **Frachon L, Mayjonade B, Bartoli C, Hautekèete N-C, Roux F.** 2019. Adaptation to plant
908 communities across the genome of *Arabidopsis thaliana*. Molecular Biology & Evolution **36**,
909 1442–1456.
910 **Freudenthal, JA, Ankenbrand, MJ, Grimm, DG, & Korte, A.** 2019. GWAS-Flow: A GPU
911 accelerated framework for efficient permutation based genome-wide association studies.
912 *BioRxiv.* doi: 10.1101/783100.
913 **Ge SX, Jung D, Yao R.** 2020. ShinyGO: a graphical gene-set enrichment tool for animals and plants.
914 Bioinformatics **36**, 2628–2629.
915 **Gomaa NH, Montesinos-Navarro A, Alonso-Blanco C, Picó FX.** 2011. Temporal variation in
916 genetic diversity and effective population size of Mediterranean and subalpine *Arabidopsis*
917 *thaliana* populations. Molecular Ecology **20**, 3540–3554.
918 **Grime, JP.** 1974. Vegetation classification by reference to strategies. Nature **250**, 26–31.
919
920 **Grime JP.** 1977. Evidence for the existence of three primary strategies in plants and its relevance to
921 ecological and evolutionary theory. The American Naturalist **111**, 1169–1194.
922 **Groszmann M, Osborn HL, Evans JR.** 2017. Carbon dioxide and water transport through plant
923 aquaporins. Plant, Cell & Environment **40**, 938–961.

924 **Gusev A, Ko A, Shi H, Bhatia G, Chung W, Penninx BWJH, Jansen R, de Geus EJC, Boomsma**
925 **DI, Wright FA, *et al.*** 2016. Integrative approaches for large-scale transcriptome-wide
926 association studies. Nature Genetics **48**, 245–252.
927 **Haldrup A, Naver H, Scheller HV.** 1999. The interaction between plastocyanin and photosystem I
928 is inefficient in transgenic Arabidopsis plants lacking the *PSI-N* subunit of photosystem I. The
929 Plant Journal **17**, 689–698.
930 **Harrell Jr F, Dupont C.** 2019. Package 'Hmisc'. CRAN2018 2019: 235–6.
931 **Heinsch FA, Reeves M, Votava P, Kang S, Milesi C, Zhao M, Glassy J, Jolly WM, Loehman R,**
932 **Bowker CF, *et al.*** 2003. Gpp and npp (mod17a2/a3) products nasa modis land algorithm.
933 MOD17 User's Guide 1–57.
934 **Hou, B, Lim, EK, Higgins, GS, Bowles, DJ.** 2004. N-glucosylation of cytokinins by
935 glycosyltransferases of Arabidopsis thaliana. *Journal of Biological Chemistry*, ***279***, 47822-
936 47832.
937 **Huang, L, He, B, Chen, A, Wang, H, Liu, J, Lű, A, & Chen, Z.** 2016. Drought dominates the
938 interannual variability in global terrestrial net primary production by controlling semi-arid
939 ecosystems. Scientific reports ***6***, 1-7.
940 **Ifuku K, Endo T, Shikanai T, Aro E-M.** 2011. Structure of the chloroplast NADH dehydrogenase-
941 like complex: nomenclature for nuclear-encoded subunits. Plant & Cell Physiology **52**, 1560–
942 1568.
943 **IRRI.** 2021. Phenotyping protocols for abiotic stress tolerance in rice. International Rice Research
944 Institute, Los Baños, Phillipines.
945 **Juenger TE, McKay JK, Simms EI, Richards JH.** 2005. Identification and characterization of QTL
946 underlying whole-plant physiology in *Arabidopsis thaliana*: $\delta^{13}C$, stomatal conductance and
947 transpiration efficiency. Plant, Cell & Environment **28**, 697–708.
948 **Karijolich, J., Yi, C., & Yu, Y. T.** 2015. Transcriptome-wide dynamics of RNA
949 pseudouridylation. Nature reviews Molecular cell biology, **16**, 581-585.
950 **Kasuga M, Liu Q, Miura S, Yamaguchi-Shinozaki K, Shinozaki K.** 1999. Improving plant
951 drought, salt, and freezing tolerance by gene transfer of a single stress-inducible transcription
952 factor. Nature Biotechnology **17**, 287–291.
953 **Kawakatsu T, Huang S-SC, Jupe F, Sasaki E, Schmitz RJ, Urich MA, Castanon R, Nery JR,**
954 **Barragan C, He Y, *et al.*** 2016. Epigenomic diversity in a global collection of *Arabidopsis*

955 *thaliana* accessions. Cell **166**: 492–505.
956 **Kim J, Rudella A, Ramirez Rodriguez V, Zybailov B, Olinares PDB, van Wijk KJ.** 2009.
957 Subunits of the plastid ClpPR protease complex have differential contributions to
958 embryogenesis, plastid biogenesis, and plant development in Arabidopsis. The Plant Cell **21**,
959 1669–1692.
960 **Kimball S, Gremer JR, Angert AL, Huxman TE, Venable DL.** 2012. Fitness and physiology in a
961 variable environment. Oecologia ***169***, 319–329.
962 **Van Kleunen M, Fischer M.** 2005. Constraints on the evolution of adaptive phenotypic plasticity in
963 plants. New Phytologist **166**, 49–60.
964 **Köhler C, Merkle T, Neuhaus G.** 1999. Characterisation of a novel gene family of putative cyclic
965 nucleotide- and calmodulin-regulated ion channels in *Arabidopsis thaliana*. The Plant Journal
966 **18**, 97–104.
967 **Korte A, Farlow A.** 2013. The advantages and limitations of trait analysis with GWAS: a review.
968 Plant Methods **9**, 29.
969 **Kramer, MC, Janssen, KA, Palos, K, Nelson AD, Vandivier LE, Garcia BA, ..., Gregory BD.**
970 2020. N6-methyladenosine and RNA secondary structure affect transcript stability and
971 protein abundance during systemic salt stress in Arabidopsis. e00239
972 **Kremling KAG, Diepenbrock CH, Gore MA, Buckler ES, Bandillo NB.** 2019. Transcriptome-
973 wide association supplements genome-wide association in *Zea mays*. G3: Genes, Genomes,
974 Genetics **9**, 3023–3033.
975 **Lasky JR, Des Marais DL, Lowry DB, Povolotskaya I, McKay JK, Richards JH, Keitt TH,**
976 **Juenger TE.** 2014. Natural variation in abiotic stress responsive gene expression and local
977 adaptation to climate in *Arabidopsis thaliana*. Molecular Biology and Evolution **31**, 2283–
978 2296.
979 **Lermontova, I, Schubert, V, Börnke, F, Macas, J, & Schubert, I.** 2007. Arabidopsis CBF5
980 interacts with the H/ACA snoRNP assembly factor NAF1. Plant molecular biology ***65***, 615-
981 626.
982 **Leyser HM, Pickett FB, Dharmasiri S, Estelle M.** 1996. Mutations in the *AXR3* gene of
983 Arabidopsis result in altered auxin response including ectopic expression from the *SAUR-AC1*
984 promoter. The Plant Journal **10**, 403–413.
985 **Li Z-G, Chen H-W, Li Q-T, Tao J-J, Bian X-H, Ma B, Zhang W-K, Chen S-Y, Zhang J-S.** 2015.

986 Three SAUR proteins *SAUR76*, *SAUR77* and *SAUR78* promote plant growth in Arabidopsis.
987 Scientific Reports **5**, 12477.
988 **Li D, Liu Q, & Schnable, PS.** 2021. TWAS results are complementary to and less affected by
989 linkage disequilibrium than GWAS. Plant Physiology **186**, 1800-1811.
990 **Liu J, Zhang Y, Qin G, Tsuge T, Sakaguchi N, Luo G, Sun K, Shi D, Aki S, Zheng N, Aoyama**
991 **T.** 2008. Targeted degradation of the cyclin-dependent kinase inhibitor ICK4/KRP6 by
992 RING-type E3 ligases is essential for mitotic cell cycle progression during Arabidopsis
993 gametogenesis. *The Plant Cell*, ***20***,1538-1554.
994 **Livingston AK, Cruz JA, Kohzuma K, Dhingra A, Kramer DM.** 2010. An Arabidopsis mutant
995 with high cyclic electron flow around photosystem I (*hcef*) involving the NADPH
996 dehydrogenase complex. Plant Cell **22**, 221–233.
997 **Lobo JM, Castro I, Moreno JC.** 2001. Spatial and environmental determinants of vascular plant
998 species richness distribution in the Iberian Peninsula and Balearic Islands. Biological Journal
999 of the Linnean Society **73**, 233–253.
1000 **Maiwald D, Dietzmann A, Jahns P, Pesaresi P, Joliot P, Joliot A, Levin JZ, Salamini F, Leister**
1001 **D.** 2003. Knock-out of the genes coding for the Rieske protein and the ATP-synthase delta-
1002 subunit of Arabidopsis. Effects on photosynthesis, thylakoid protein composition, and nuclear
1003 chloroplast gene expression. Plant Physiology **133**, 191–202.
1004 **Manzano-Piedras E, Marcer A, Alonso-Blanco C, Picó FX.** 2014. Deciphering the adjustment
1005 between environment and life history in annuals: lessons from a geographically-explicit
1006 approach in *Arabidopsis thaliana*. PLoS One 9, e87836.
1007 **Marcer A, Vidigal DS, James PMA, Fortin MJ, Méndez-Vigo B, Hilhorst HWM, Bentsink L,**
1008 **Alonso-Blanco C, Picó FX.** 2018. Temperature fine-tunes Mediterranean *Arabidopsis*
1009 *thaliana* life-cycle phenology geographically. Plant Biology **20**, 148–156.
1010 **Méndez-Vigo B, Picó FX, Ramiro M, Martínez-Zapater JM, Alonso-Blanco C.** 2011. Altitudinal
1011 and climatic adaptation is mediated by flowering traits and FRI, FLC, and PHYC genes in
1012 Arabidopsis. Plant Physiology **157**, 1942–1955.
1013 **Montesinos A, Tonsor SJ, Alonso-Blanco C, Picó FX.** 2009. Demographic and genetic patterns of
1014 variation among populations of *Arabidopsis thaliana* from contrasting native environments.
1015 PLoS One 4, e7213.
1016 **Montesinos-Navarro A, Wig J, Pico FX, Tonsor SJ.** 2011. *Arabidopsis thaliana* populations show

1017 clinal variation in a climatic gradient associated with altitude. New Phytologist **189**, 282–294.
1018 **Murakami R, Ifuku K, Takabayashi A, Shikanai T, Endo T, Sato F.** 2005. Functional dissection
1019 of two Arabidopsis PsbO proteins: *PsbO1* and *PsbO2*. The FEBS Journal **272**, 2165–2175.
1020 **Nagatoshi Y, Ikeda M, Kishi H, Hiratsu K, Muraguchi A, Ohme-Takagi M.** 2016. Induction of
1021 a dwarf phenotype with IBH1 may enable increased production of plant-made
1022 pharmaceuticals in plant factory conditions. Plant Biotechnology Journal **14**, 887–894.
1023 **Nilson, S. E., & Assmann, S. M.** 2010. Heterotrimeric G proteins regulate reproductive trait
1024 plasticity in response to water availability. New Phytologist **185***,* 734-746.
1025 **Nishimura K, van Wijk KJ.** 2015. Organization, function and substrates of the essential Clp
1026 protease system in plastids. *Biochimica et Biophysica Acta* **1847**, 915–930.
1027 **Oh E, Zhu J-Y, Bai M-Y, Arenhart RA, Sun Y, Wang Z-Y.** 2014. Cell elongation is regulated
1028 through a central circuit of interacting transcription factors in the Arabidopsis hypocotyl.
1029 Elife. doi: 10.7554/eLife.03031.
1030 **Ohashi-Ito K, Matsukawa M, Fukuda H.** 2013. An atypical bHLH transcription factor regulates
1031 early xylem development downstream of auxin. Plant Cell Physiol **54**, 398–405.
1032 **Park SY, Scranton MA, Stajich JE, Yee A, Walling LL.** 2017. Chlorophyte aspartyl
1033 aminopeptidases: ancient origins, expanded families, new locations, and secondary
1034 functions. Plos one ***12***, p.e0185492.
1035 **Parsons RF.** 1968. The significance of growth-rate comparisons for plant ecology. The American
1036 Naturalist **102**, 595–597.
1037 **Páscoa P, Gouveia CM, Russo A, Trigo RM.** 2017. Drought Trends in the Iberian Peninsula over
1038 the Last 112 Years. Advances in Meteorology **2017**, 1–13.
1039 **Picó FX.** 2012. Demographic fate of *Arabidopsis thaliana* cohorts of autumn- and spring-germinated
1040 plants along an altitudinal gradient. Journal of Ecology **100**, 1009–1018.
1041 **Picó FX, Méndez-Vigo B, Martínez-Zapater JM, Alonso-Blanco C.** 2008. Natural genetic
1042 variation of *Arabidopsis thaliana* is geographically structured in the Iberian peninsula.
1043 Genetics **180**, 1009–1021.
1044 **Price AL, Zaitlen NA, Reich D, Patterson N.** 2010. New approaches to population stratification in
1045 genome-wide association studies. Nature Reviews Genetics **11**, 459–463.
1046 **Rey Benayas JM, Scheiner SM.** 2002. Plant diversity, biogeography and environment in Iberia:
1047 Patterns and possible causal factors. Journal of Vegetation Science **13**, 245.

1048 **Rivero RM, Kojima M, Gepstein A, Sakakibara H, Mittler R, Gepstein S, Blumwald E.** 2007.
1049 Delayed leaf senescence induces extreme drought tolerance in a flowering plant. Proceedings
1050 of the National Academy of Sciences **104**,19631-19636.
1051 **Running SW, Zhao M.** 2015. Daily GPP and annual NPP . MOD17A2/A3. products NASA Earth
1052 Observing System MODIS land algorithm. MOD17 User's Guide 2015, 1–28.
1053 **Salehin M, Li B, Tang M, Katz E, Song L, Ecker JR, Kliebenstein DJ, Estelle M.** 2019. Auxin-
1054 sensitive Aux/IAA proteins mediate drought tolerance in Arabidopsis by regulating
1055 glucosinolate levels. Nature Communications **10**, 4021.
1056 **Schindele A, Dorn A, Puchta H.** 2020. CRISPR/Cas brings plant biology and breeding into the fast
1057 lane. Current Opinion in Biotechnology **61**, 7–14.
1058 **Schweizer F, Fernández-Calvo P, Zander M, Diez-Diaz M, Fonseca S, Glauser G, Lewsey MG,**
1059 **Ecker JR, Solano R, Reymond P.** 2013. Arabidopsis basic helix-loop-helix transcription
1060 factors MYC2, MYC3, and MYC4 regulate glucosinolate biosynthesis, insect performance,
1061 and feeding behavior. Plant Cell **25**, 3117–3132.
1062 **Seren Ü, Vilhjálmsson BJ, Horton MW, Meng D, Forai P, Huang YS, Long Q, Segura V,**
1063 **Nordborg M.** 2012. GWAPP: a web application for genome-wide association mapping in
1064 Arabidopsis. Plant Cell **24**, 4793–4805.
1065 **Togninalli M, Seren Ü, Freudenthal JA, Monroe JG, Meng D, Nordborg M, Borgwardt K,**
1066 **Grimm, DG.** 2020. AraPheno and the AraGWAS Catalog 2020: a major database update
1067 including RNA-Seq and knockout mutation data for Arabidopsis thaliana. Nucleic acids
1068 research, **48**, D1063-D1068.
1069 **Siepielski AM, Morrissey MB, Buoro M, Carlson SM, Caruso CM, Clegg SM, Coulson T,**
1070 **DiBattista J, Gotanda KM, Francis CD, *et al.*** 2017. Precipitation drives global variation in
1071 natural selection. Science **355**, 959–962.
1072 **Spartz AK, Ren H, Park MY, Grandt KN, Lee SH, Murphy AS, Sussman MR, Overvoorde PJ,**
1073 **Gray WM.** 2014. SAUR inhibition of PP2C-D Phosphatases activates plasma membrane H^+-
1074 ATPases to promote cell expansion in Arabidopsis. Plant Cell **26**, 2129–2142
1075 **Stortenbeker N, Bemer M. 2019.** The SAUR gene family: the plant's toolbox for adaptation of
1076 growth and development. Journal of Experimental Botany **70**, 17–27.
1077 **Tabas-Madrid D, Méndez-Vigo B, Arteaga N, Marcer A, Pascual-Montano A, Weigel D, Xavier**
1078 **Picó F, Alonso-Blanco C.** 2018. Genome-wide signatures of flowering adaptation to climate

1079 temperature: regional analyses in a highly diverse native range of *Arabidopsis thaliana*. Plant,
1080 Cell & Environment **41**, 1806–1820.
1081 **Tang, Y., Gao, C. C., Gao, Y., Yang, Y., Shi, B., Yu, J. L., ... & Chong, K.** 2020. OsNSUN2-
1082 mediated 5-methylcytosine mRNA modification enhances rice adaptation to high
1083 temperature. Developmental cell ***53***, 272-286.
1084 **Team RC.** 2013. R: A language and environment for statistical computing.
1085 **The 1001 Genomes Consortium** 2016. 1,135 Genomes reveal the global pattern of polymorphism
1086 in *Arabidopsis thaliana*. Cell **166**, 481–491.
1087 **Tilman D.** 1988. Plant strategies and the dynamics and structure of plant communities. Princeton
1088 University Press.
1089 **Tunc-Ozdemir M, Tang C, Ishka MR, Brown E, Groves NR, Myers CT, Rato C, Poulsen LR,**
1090 **McDowell S, Miller G, *et al*.** 2013. A cyclic nucleotide-gated channel (CNGC16) in pollen
1091 is critical for stress tolerance in pollen reproductive development. Plant Physiology **161**,
1092 1010–1020.
1093 **Via S, Gomulkiewicz R, De Jong G, Scheiner SM, Schlichting CD, Van Tienderen PH.** 1995.
1094 Adaptive phenotypic plasticity: consensus and controversy. Trends in Ecology & Evolution.
1095 **10,** 212–217.
1096 **Vicente-Serrano SM.** 2006a. Spatial and temporal analysis of droughts in the Iberian Peninsula.
1097 1910–2000. Hydrological Sciences Journal **51**, 83–97
1098 **Vicente-Serrano SM.** 2006b. Differences in spatial patterns of drought on different time scales: an
1099 analysis of the iberian peninsula. Water Resources Management **20**, 37–60.
1100 **Vidigal DS, Marques ACSS, Willems LAJ, Buijs G, Méndez-Vigo B, Hilhorst HWM, Bentsink**
1101 **L, Picó FX, Alonso-Blanco C.** 2016. Altitudinal and climatic associations of seed dormancy
1102 and flowering traits evidence adaptation of annual life cycle timing in *Arabidopsis thaliana*.
1103 Plant, Cell & Environment **39**, 1737–1748.
1104 **Wang Y-F, Munemasa S, Nishimura N, Ren H-M, Robert N, Han M, Puzõrjova I, Kollist H,**
1105 **Lee S, Mori I, *et al*.** 2013. Identification of cyclic GMP-activated nonselective Ca2+-
1106 permeable cation channels and associated *CNGC5* and *CNGC6* genes in Arabidopsis guard
1107 cells. Plant Physiology **163**, 578–590.
1108 **Wang Z, Yang L, Liu Z, Lu M, Wang M, Sun Q, Lan Y, Shi T, Wu D, Hua J.** 2019. Natural
1109 variations of growth thermo-responsiveness determined by SAUR26/27/28 proteins in

1110 *Arabidopsis thaliana*. New Phytologist **224**, 291–305.
1111 **Wang Z, Yang L, Wu D, Zhang N, Hua J.** 2021. Polymorphisms in cis-elements confer SAUR26
1112 gene expression difference for thermo-response natural variation in Arabidopsis. New
1113 Phytologist **229**, 2751–2764.
1114 **Weijschedé, J, Martínková, J, De Kroon, H, & Huber, H.** 2006. Shade avoidance in *Trifolium*
1115 *repens*: costs and benefits of plasticity in petiole length and leaf size. New Phytologist ***172,***
1116 655-666.
1117 **West-Eberhard MJ.** 2003. Developmental plasticity and evolution. Oxford University Press
1118 **Wickham H, Francois R, Henry L, Müller K.** 2015. dplyr: A grammar of data manipulation. R
1119 package version 0.4 3.
1120 **Wickham H, Henry L.** 2018. tidyr: Easily Tidy Data with 'spread 'and 'gather'Functions. R package
1121 version 0.8 2.
1122 **Wolfe MD, Tonsor SJ.** 2014. Adaptation to spring heat and drought in northeastern Spanish
1123 *Arabidopsis thaliana*. New Phytologist **201**, 323–334.
1124 **Wong JH, Klejchová M, Snipes SA, Nagpal P, Bak G, Wang B, ..., Gray WM.** 2021. SAUR
1125 proteins and PP2C. D phosphatases regulate H^+-ATPases and K+ channels to control
1126 stomatal movements. Plant Physiology **185**, 256-273.
1127 **Yamori W, Sakata N, Suzuki Y, Shikanai T, Makino A.** 2011. Cyclic electron flow around
1128 photosystem I via chloroplast NAD. P.H dehydrogenase. NDH. complex performs a
1129 significant physiological role during photosynthesis and plant growth at low temperature in
1130 rice. Plant Journal **68**, 966–976.
1131 **Zait Y, Ferrero-Serrano Á & Assmann, SM.** 2021. The α subunit of the heterotrimeric G protein
1132 regulates mesophyll CO_2 conductance and drought tolerance in rice. New Phytologist, **232**,
1133 2324-2338.
1134 **Zhang, J, Vankova, R, Malbeck, J, Dobrev, PI, Xu, Y, Chong, K, Neff, MM.** 2009. *AtSOFL1* and
1135 *AtSOFL2* act redundantly as positive modulators of the endogenous content of specific
1136 cytokinins in Arabidopsis. *PLoS One*, ***4***, p.e8236.
1137 **Zhang H, Zhao Y, Zhu J-K.** 2020. Thriving under stress: how plants balance growth and the stress
1138 response. Developmental Cell **55**, 529–543.
1139 **Zhao Z, Zhang W, Stanley BA, Assmann SM.** 2008. Functional proteomics of *Arabidopsis thaliana*
1140 guard cells uncovers new stomatal signaling pathways. The Plant Cell, **20**, 3210-26.

1141 **Zheng Q, Zheng Y, Ji H, Burnie W, Perry SE.** 2016. Gene regulation by the *AGL15* transcription
1142 factor reveals hormone interactions in somatic embryogenesis. Plant Physiology **172**, 2374–
1143 2387.
1144
1145

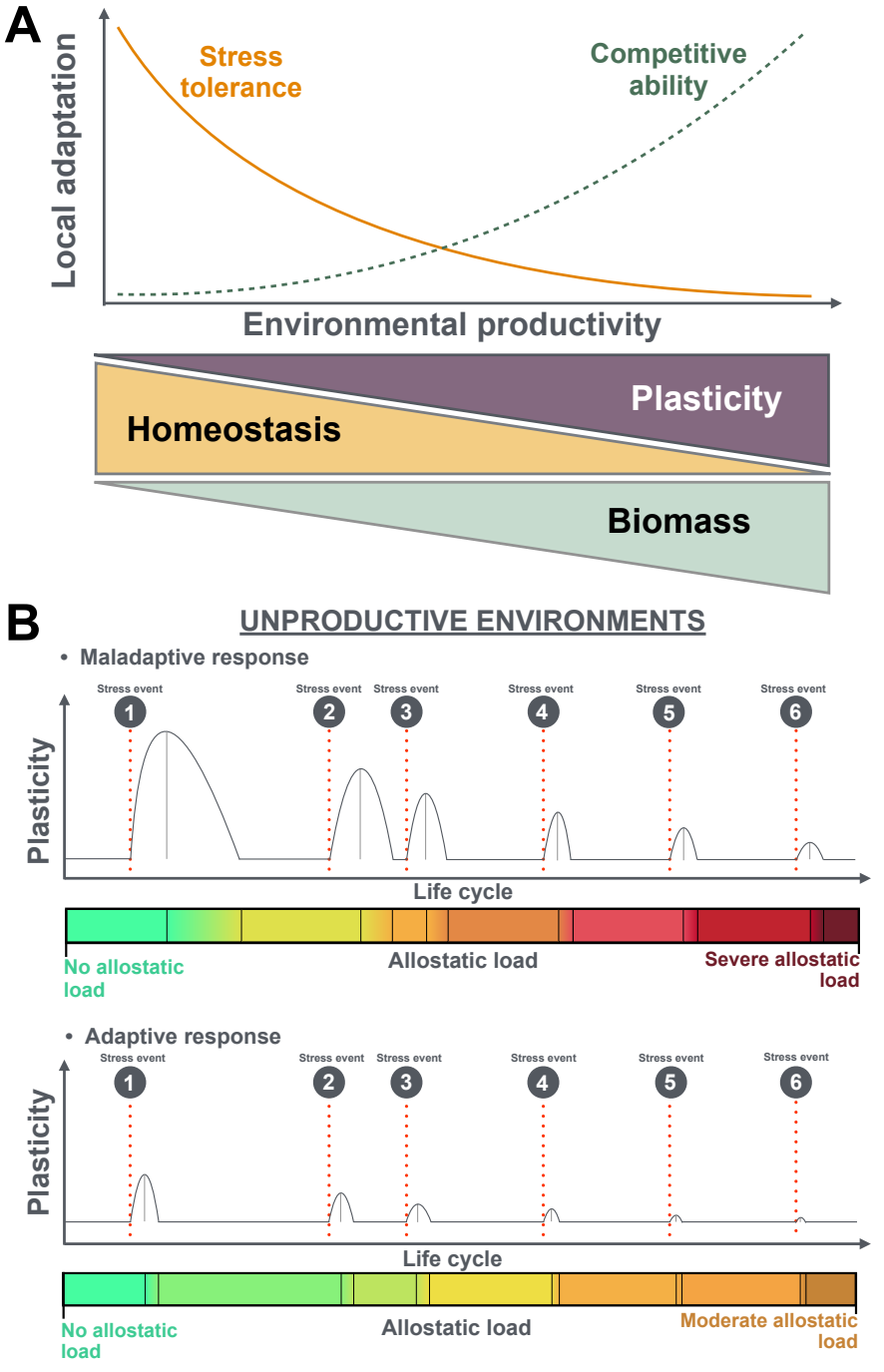

Fig 1. Conceptual framework for the adaptive role of plastic and homeostatic responses across productivity gradients in the local environment. (A) Schematic illustration representing the balance *sensu* Grime (1974, 1977), between stress tolerance in lower productivity, stress-prone environments, and competitive ability in and homeostasis in plants. In less productive environments, homeostatic responses to stress and lower relative growth rates result in lower biomass production, which is tuned in to the lower resources that are typically available in their environment and favors adaptation to those environments. In contrast, in productive environments, in which competition becomes more intense, plastic responses are favored from an adaptive standpoint. (B). In unproductive environments, frequent stress events can increase the allostatic load in individuals adapted to high-productivity environments where plastic responses are beneficial. During the lifetime of an individual, this results in a maladaptive response that increases allostatic load. In contrast, individuals adapted to unproductive environments exhibit less plastic (more homeostatic) responses to repeated stress that reduces their allostatic load over their lifetime.

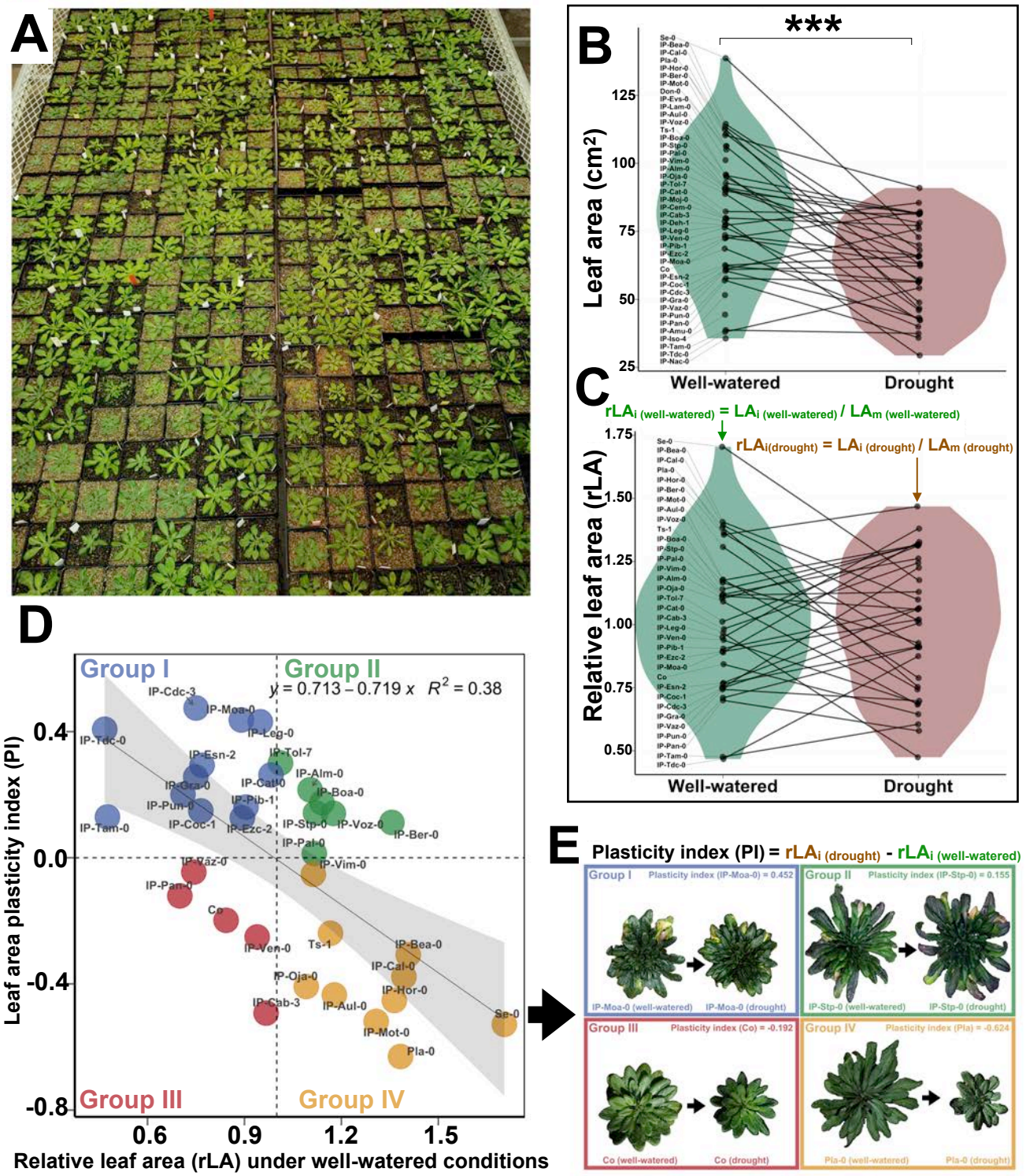

Fig. 2. Accession-specific rosette leaf area responses in Arabidopsis. (A) Detail of the common garden experiment, illustrating the randomization of well-watered and drought treatments, as reflected in soil coloration. (B) Phenotypic reaction norms illustrating a reduction of leaf area in response to drought in most but not all accessions. Violin distributions represent probability densities of leaf area (cm^2) among the accessions included in this study. Datapoints depict the mean phenotypic values of individual accessions, and the reaction norms represent the plastic response in the leaf area of each accession in response to drought (t-test; P-value < 0.001). (C) Phenotypic reaction norms illustrating plastic and homeostatic responses in relative leaf area (rLA). Violin distributions represent probability densities of rLA among the accessions included in this study. Datapoints depict the rLA of individual accessions, and the reaction norms represent the plastic response in rLA of each accession in response to drought (t-test; P-value > 0.05). (D) Negative relationship (P-value < 0.05) between leaf area plasticity index (slope of the reaction norms in 2C) in response to drought (y-axis) and rLA under well-watered conditions (x-axis). Data were fitted using a linear regression model. Grey shadow represents the 95% CI of the fit regression line. Four different quadrants are defined by two dashed lines: the average rLA (x-axis), and y = 0, which is the homeostatic point at which a change in water availability does not affect rLA (i.e. a plasticity index of 0). Data points depict individual accessions with their respective label. Data points are colored based on in which quadrant they fall (see text). (E) Images illustrating the plastic and homeostatic responses to drought found among the accessions included in this study.

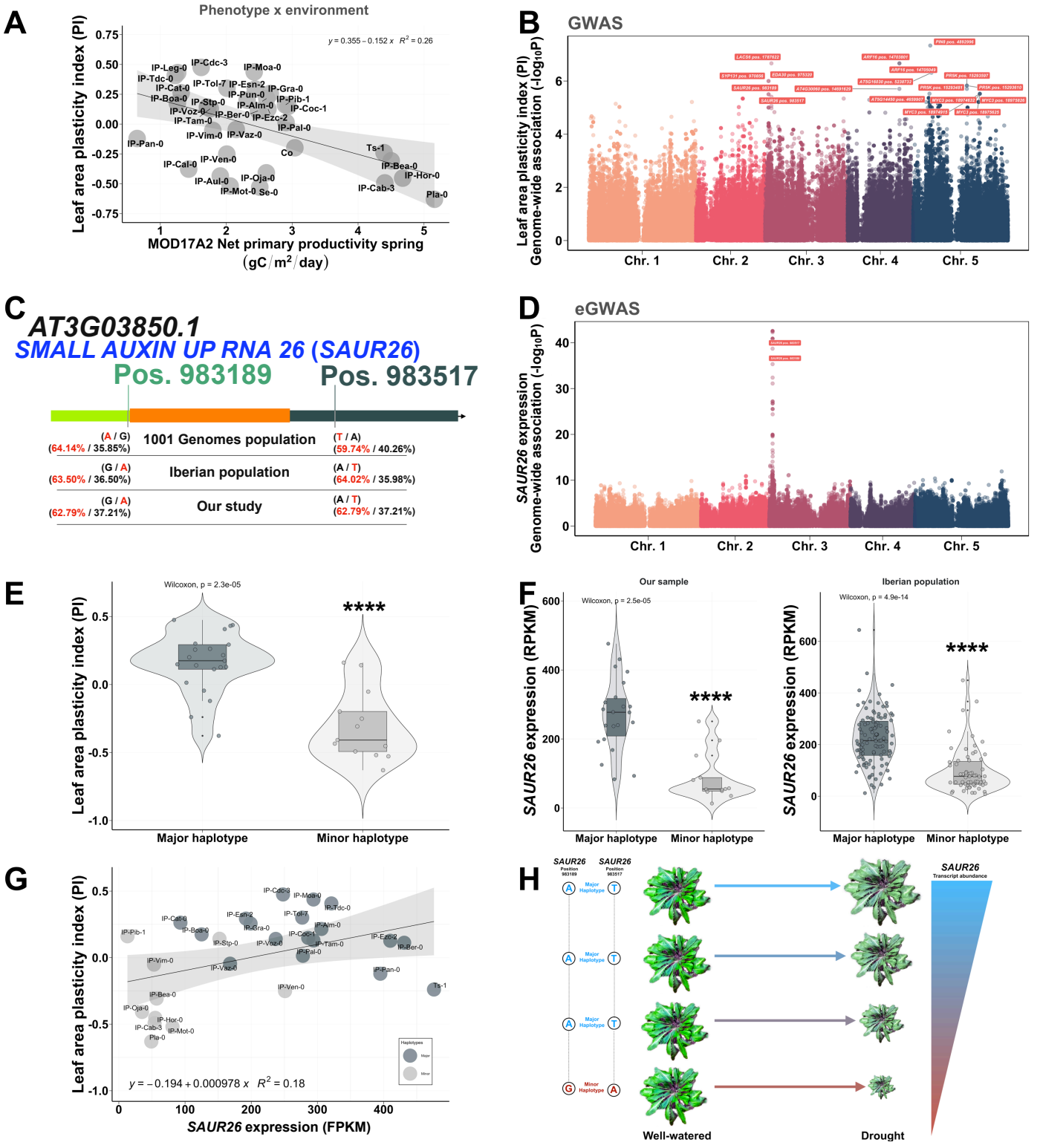

Fig. 3. *SMALL AUXIN UP RNA 26* (*SAUR26,* AT3G03850) is a candidate regulator of Arabidopsis leaf area plasticity in response to drought. (A) Accessions from more productive areas display stronger negative reductions in leaf area plasticity relative to accessions from less productive environments. Scatter plot depicting the negative relationship (P-value < 0.05) between leaf area plasticity index (y-axis) and Net Primary Productivity during the spring season (x-axis). (B) Manhattan plot representing the strength of association between genetic variants and leaf area plasticity in response to drought. (C) *SAUR26* gene model, including the two co-varying SNPs highlighted in 2B. Orange block depicts the sole exon, green block the 5' UTR, dark green block the 3' UTR. Labels above indicate the position of the two SNPs that co-vary, forming a haplotype in our sample. Major/minor allele frequency in our sample, in the 189 accessions from the Iberian Peninsula included in the 1001 Genome Project, and the whole 1001 Genomes Project sample dataset is provided. (D) Manhattan plot representing the genome-wide strength of association between the genetic variation present within the 665 accessions from the transcript abundance reference panel (Kawakatsu *et al.*, 2016) that overlap with the collection of accessions included in the 1001 Genomes Project, and the variation in the transcript abundance of *SAUR26* (Kawakatsu *et al.*, 2016). The peak in chromosome 3 represents the cis-genetic variants in *SAUR26* affecting its transcript abundance. For the Manhattan plots in 3B and D, the score (y-axis) consists of the negative logarithm of the P-value and provides association strength. Each data point represents a SNP with a color corresponding to the chromosome where the genetic variants are located. The x-axis and the different colors shown in the SNPs depicted in the Manhattan plots represent the different chromosomes. The higher the score, the lower the P-value, and the stronger the association between genetic variation and leaf area plasticity or *SAUR26* transcript abundance. (E) In the Iberian population, the major haplotype of *SAUR26* is associated with homeostatic or positive responses of relative leaf area (rLA) in response to drought. Conversely, the minor haplotype in the Iberian population is associated with plastic responses in rLA in response to drought. Violin plots show significantly different probability densities of leaf area plasticity in response to drought for the major and minor allele haplotypes in *SAUR26.* (F) The haplotypes in *SAUR26* associated with leaf area plasticity/homeostasis in response to drought are associated with differences in *SAUR26* gene expression. Violin plots show significantly different probability densities of *SAUR26* transcript abundance for the major and minor allele haplotypes in *SAUR26* for both our sample and the entire Iberian population. (G) Scatter plot illustrating the positive relationship between leaf area plasticity index (y-axis) and *SAUR26* transcript abundance (x-axis). For 2A and 2G, the grey shadow represents the 95% CI of the fit regression line (dark grey). (H) Cartoon illustrating the regulatory role of genetic and transcript variation in *SAUR26* and the response of leaf area to drought.

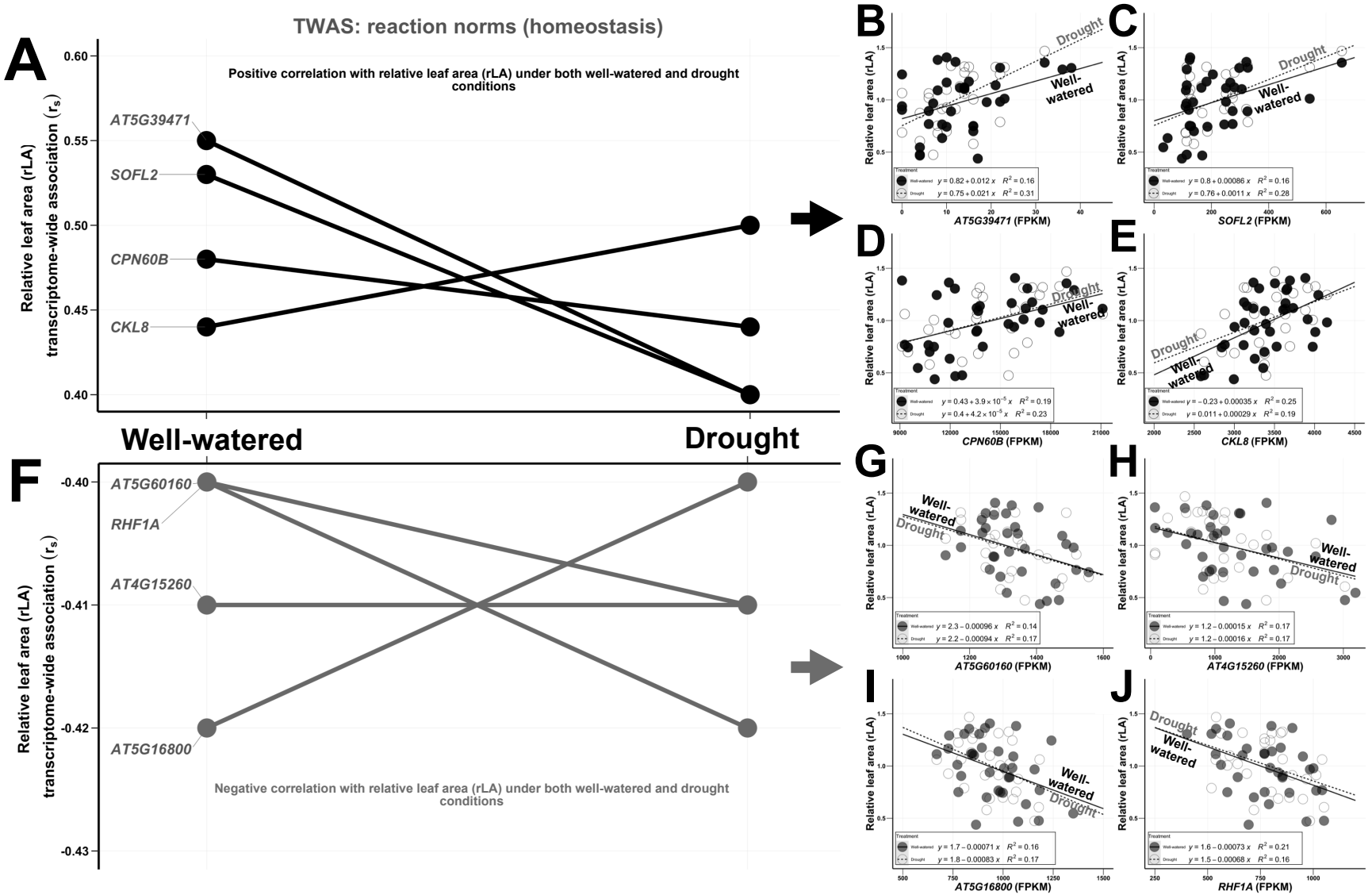

Fig. 4. Transcriptomic reaction norms uncover genetic correlates of Arabidopsis leaf area homeostasis in response to drought. (A) homeostatic reaction norms for transcripts significantly and positively correlated with relative leaf area (rLA) under both watering regimes. (B) to (E). Scatter plots illustrating positive and homeostatic relationships (P-value < 0.05) between rLA under both well-watered (closed circles) and drought conditions (open circles) conditions (y-axis), and transcript abundance (FPKM; x-axis) of (B) AT5G39471, (C) *SOB FIVE-LIKE 2* (*SOFL2; AT1G68870*)**,** (D) *CHAPERONIN 60 BETA* (*CPN60B*; *AT1G55490*), and (E) *CASEIN KINASE I-LIKE 8* (*CKL8*; *AT5G43320*). (F) homeostatic reaction norms for transcripts significantly and negatively correlated with rLA under both watering regimes. (G) to (J) Scatter plots illustrating negative and homeostatic relationships (P-value < 0.05) between rLA under both well-watered (closed circles) and drought conditions (open circles) (y-axis), and transcript abundance (FPKM; x-axis) of (G) AT5G60160, (H) *AT4G15260***,** (I) *AT5G16800*, and (J) *RING-H2 GROUP F1A* (*RHF1A*; *AT4G14220*). For 3a and 3f, Spearman's rank correlation coefficient ($r_{s;}$ y-axis) indicates the correlation between the rLA and the natural variation in transcript abundance of each gene. In Figs B to E and G to J, data were fitted using a linear regression model. Also, in panels b-e and g-j, filled circles depict the rLA of accessions grown under well-watered conditions, while empty circles squares depict the rLA of accessions grown under drought.

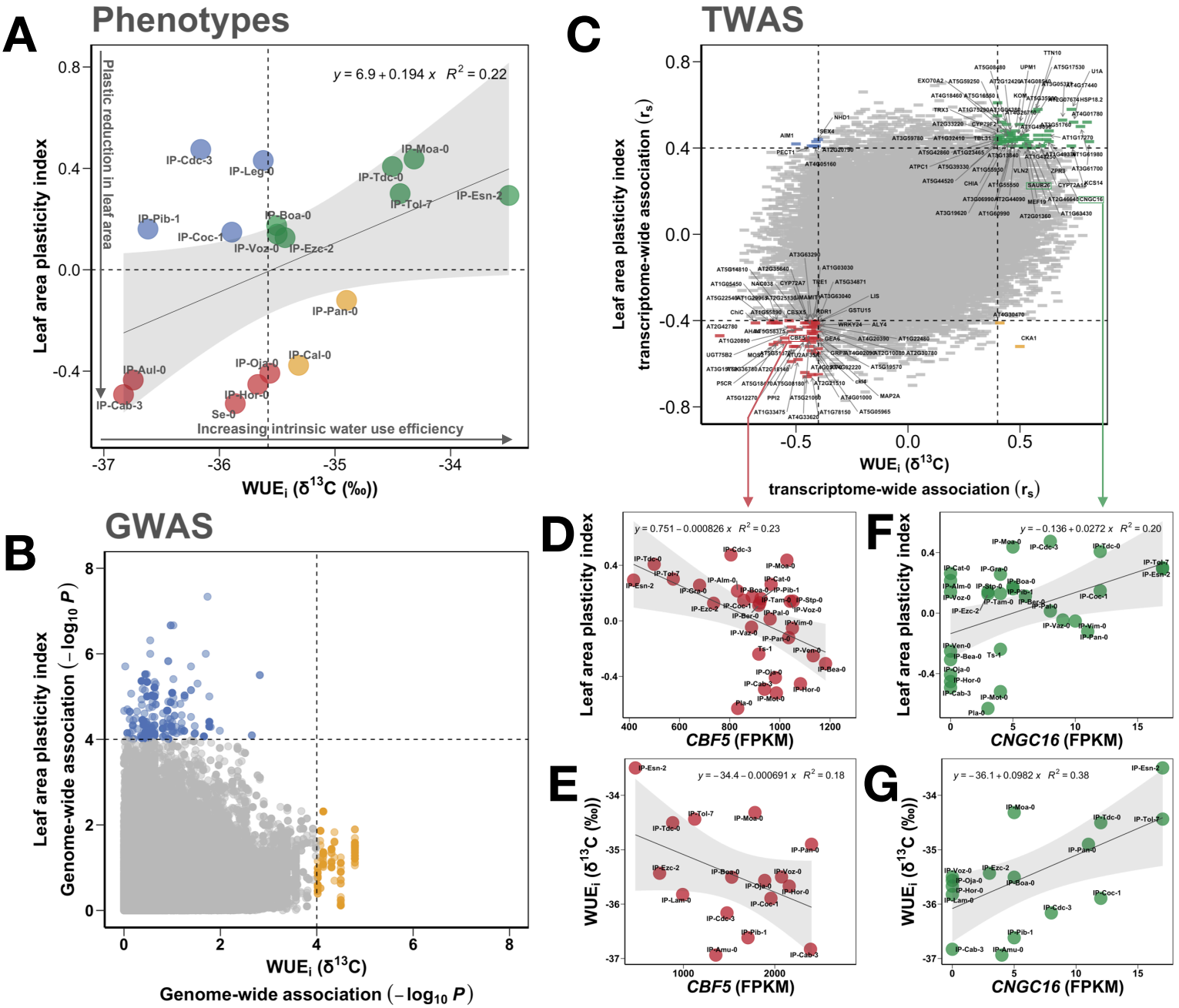

Fig. 5. Arabidopsis accessions that display leaf area homeostasis in response to drought, display higher water use efficiency as defined by $\delta^{13}C$. **(A)** Scatter plot illustrating the positive relationship (P-value < 0.05) between leaf area homeostasis in response to drought (leaf area plasticity index, y-axis) and water use efficiency (x-axis) among Iberian Arabidopsis accessions used in this study. Data were fitted to a linear regression model. Grey shadow represents the 95% CI of the fit regression line (black). $\delta^{13}C$ data for the accessions were retrieved from Dittberner *et al.* (2018). Four different quadrants are defined by two dashed lines: y = 0, which is the homeostatic point at which a change in water availability does not affect relative leaf area (i.e., a plasticity index of 0), and the average intrinsic water use efficiency (WUE_i, $\delta^{13}C$; x-axis). Data points depict individual accessions with their respective labels. **(B)** The genetic basis of leaf area plasticity in response to drought and water use efficiency. This plot depicts the respective relationship between the GWAS associations found for the leaf area plasticity index in response to drought (y-axis) and those for WUE_i (Dittberner *et al.*, 2018) (x-axis). Data points represent individual SNPs. The y-axis and x-axis depict the extent of the association with, respectively, leaf area plasticity, and WUE_i, as the negative logarithm of the p-value. Dashed lines depict an arbitrary threshold for significance that is consistent across comparisons. (C) Transcriptomic association with plastic leaf area responses to drought and WUE_i. Spearman's rank correlation depicts the relationship between the association of the transcript abundance of each gene in the Arabidopsis genome with leaf area plasticity in response to drought (r_s) on the y-axis and with WUE_i on the x-axis. Dashed lines define an arbitrary threshold to consider transcripts correlated positively ($r_s \geq 0.4$) or negatively ($r_s \leq -0.4$) associated with leaf area plasticity (y-axis) or WUE_i (x-axis). *CBF5* and *CNGC16* exemplify transcripts with opposing relationships to leaf area plasticity and water use efficiency as shown in 4C, D and E. Scatter plots depicting the relationship (P-value < 0.05) between leaf area plasticity index in response to drought (4D), or water use efficiency (4E) on the y-axis, and transcript abundance (FPKM) of *CBF5* on the x-axis. F and G. Scatter plots depicting the relationship (P-value < 0.05) between (4F) leaf area plasticity index in response to drought or (4G) water use efficiency (Dittberner *et al.*, 2018) on the y-axis, and transcript abundance (FPKM) of *CYCLIC NUCLEOTIDE-GATED CHANNEL 16* (*CNGC16*) on the x-axis. In all panels, data were fitted using a linear regression model. Grey shadow represents the 95% CI of the fit regression line.

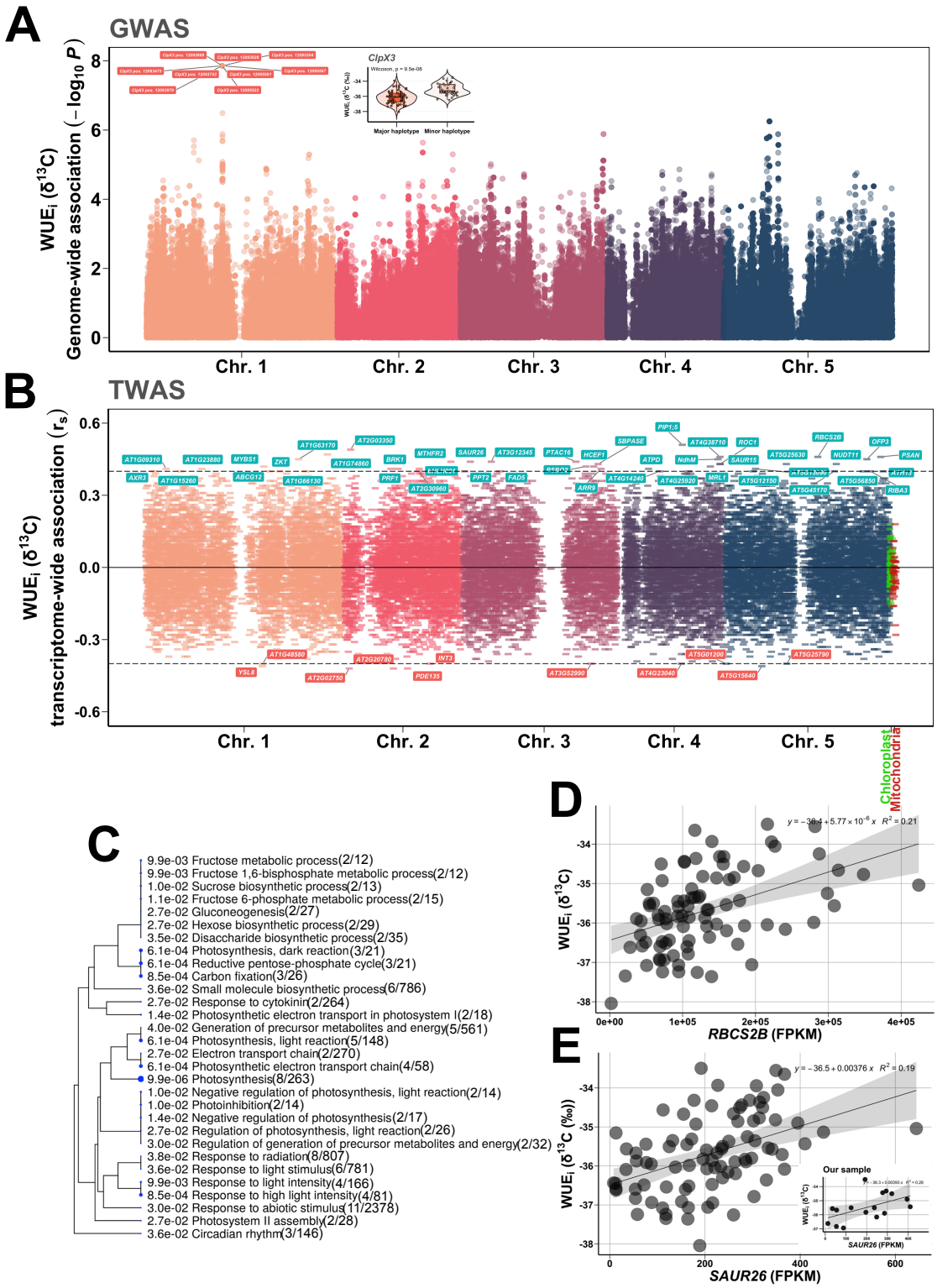

Fig. 6. Photosynthesis-related transcript variants regulate water use efficiency in Iberian Arabidopsis accessions. (A) Manhattan plot representing the genome-wide strength of association between genetic variation and variation in δ13C present within 95 Iberian accessions with δ13C values available from Dittberner *et al*. (2018). The score (y-axis) consists of the negative logarithm of the *P*-value and provides association strength. Inset: Violin plots representing the probability densities of WUE_i for the major and minor allele haplotypes in *ClpX* for the accessions included in Fig. 6A. (B) T-Manhattan plot representing transcriptome-wide strength of association between variation in transcript abundance (Kawakatsu *et al.*, 2016) and natural variation in δ13C. This analysis was performed on all Iberian accessions with both transcript abundance data (Kawakatsu *et al.*, 2016) and δ13C information (Dittberner *et al.*, 2018) (n = 88 accessions). The relationship is defined by the Spearman's rank correlation coefficient (r_s). Dashed lines define an arbitrary threshold for positive ($r_s \geq 0.4$) or negative ($r_s \leq -0.4$) correlation with water-use efficiency (y-axis). Blue labels highlight the transcripts positively associated with higher WUE_i, while red labels highlight those negatively associated with higher WUE_i. (C) Hierarchical clustering tree summarizing the correlation among significant GO Biological Process categories resulting from analysis of the positively correlated candidates resulting from TWA analysis of water use efficiency determined from δ13C values in 88 Iberian Arabidopsis accessions. Ratios provide the number of genes positively correlated with WUE_i within each GO category relative to the total number of genes within that category. The size of the blue dots increases proportionally with P-value significance. (D) Scatter plot depicting the positive relationship (*P*-value < 0.05) between WUE_i (y-axis) and *RuBisCO SMALL SUBUNIT 2B* (*AT5G38420*; *RBCS2B*) transcript abundance (x-axis) for the Iberian accessions included in Fig. 6B. (E) Scatter plot depicting the positive relationship (*P*-value < 0.05) between intrinsic water-use efficiency (WUE_i; y-axis) and *SMALL AUXIN UP RNA 26* (*SAUR26,* AT3G03850) transcript abundance (x-axis) for the Iberian accessions included in 6b. Inset: Scatter plot depicting the positive relationship (*P*-value < 0.05) between intrinsic water-use efficiency (WUE_i; y-axis) and *SMALL AUXIN UP RNA 26* (*SAUR26,* AT3G03850) transcript abundance (x-axis) for the 43 accessions included in our study. For 5D, and 5E, gray shadow represents the 95% CI of the fit regression line (black).